

# A LEVEL SET-BASED STRUCTURAL OPTIMIZATION CODE USING FENICS

ANTOINE LAURAIN

**ABSTRACT.** In this paper we present an educational code written using FEniCS, based on the level set method, to perform compliance minimization in structural optimization. We use the concept of distributed shape derivative to compute a descent direction for the compliance, which is defined as a shape functional. The use of the distributed shape derivative is facilitated by FEniCS, which allows to handle complicated partial differential equations with a simple implementation. The code is written for compliance minimization in the framework of linearized elasticity, but can be easily adapted to tackle other functionals and partial differential equations. We start by explaining the shape sensitivity analysis, recalling some tools of shape calculus, and discuss the differences between the distributed and boundary expression of the shape derivative. Then we describe the implementation in details, and show the application of this code to the classical benchmarks of topology optimization. The code can be downloaded at [http://antoinelaurain.com/recherche\\_struct\\_eng.htm](http://antoinelaurain.com/recherche_struct_eng.htm), and the main file is given in the appendix.

## 1. INTRODUCTION

The popular “99 line” Matlab code by Sigmund published in 2001 [52] has started a trend of sharing and publishing educational codes for structural optimization. Since then, an upgrade of the “99 line” code has been published, improving speed and reducing the code size to 88 lines; see [8]. The codes of [8, 52] are written for Matlab and are based on the SIMP approach [1, 10, 41]. Various other codes have been published using different approaches and/or other platforms than Matlab. We review here several categories of approaches to tackle this problem.

In the solid isotropic microstructure with penalty (SIMP) approach the material is allowed to have intermediate values, and the optimization variables are the material densities of the mesh elements. The intermediate values are also penalized using a power law to enforce 0 – 1 values. Using filtering techniques, it provides feasible designs. Considering SIMP approaches as in [52], Talischí et al. have introduced `PolyMesher` [57] and `PolyTop` [58] to provide a Matlab implementation of topology optimization using a general framework for finite element discretization and analysis. Liu and Tovar have also published a 3D code; see [37]. There are also several publications on topology optimization using GPU; see [22, 49, 65].

Another category of approaches for topology optimization which has emerged after the SIMP approach are level set methods. They consist in representing the boundary of the moving domain  $\Omega$  as the zero level set of a function  $\phi$ . Level set methods have been introduced by Osher and Sethian [44] to facilitate the modelization of topological changes during curve evolution. Since then, they have been applied to many shape optimization/ optimal design/ boundary perturbations problems. Concerning applications of level set methods to structural optimization, there is already a consequent literature, see for instance [4, 5, 51, 62, 63] for the pioneering works using this approach, and [61] for a review.

Early references for level set approaches include a code in Femlab [38] by Liu et al. in 2005. In 2010, Challis published a level set-based Matlab code [16] in the spirit of the “99 line” code. In 2014, Otomori et al. have published a Matlab code [46], also in 88 lines, for level set-based topology optimization using a reaction-diffusion equation. See also [17, 31] for implementations using GPU.

Level set methods are sometimes classified as PDE-based approaches for topology optimization. Another class of PDE-based approach which has gained interest recently are phase-field methods. The phase-field approach also allows topological changes, and does not represent the domains with a sharp but with a diffuse interface, whose thickness is proportional to a small parameter; see [12, 13, 14, 15, 48, 56, 64].

There exists other approaches to structural topology optimization. Some groups have developed level-set methods which do not involve solving the Hamilton-jacobi equation, see for instance [9, 60] and [7] for an algorithm based on the notion of topological derivative. We also mention an early `FreeFem++` code [3] by Allaire and Pantz in 2006, implementing the boundary variation method and the homogenization. For a critical comparison of four different level-set approaches and one phase-field approach to topology optimization, see [28].

The code presented in the present paper enters the category of level set methods described above. In the usual level set approach, the concept of shape derivative is used to compute the sensitivity of the objective functional; see [20, 30, 53] for an introduction to shape derivatives. It is known that the shape derivative is a distribution on the boundary of the domain under optimization, and the algorithms are usually based on this property. This means

that the shape derivative is computed on the boundary, and then extended to the entire domain or to a narrow band for use in the level set method; see [3, 4, 5, 16, 24, 25, 26, 27, 32, 33, 51, 62, 63] for applications of this approach. In fact, the shape derivative can be written as a domain integral, which is called *distributed* or *domain expression* of the shape derivative; see [11, 21, 35, 36], and [34, 42, 55] for applications. See also [59], where the relation between the distributed shape derivative and the Eshelby energy-momentum tensor concept [23] of continuum mechanics theory is analyzed, in the context of torsion of elastic shafts.

From a numerical point of view, the distributed expression is often easier to implement than the boundary expression as it is a volume integral. Other advantages of the distributed expression are shown in [11, 35]. In [11], it is shown that the discretization and the shape differentiation processes commute for the volume expression but not for the boundary expression; i.e., a discretization of the boundary expression does not generally lead to the same expression as the shape derivative computed after the problem is discretized. In [35], the authors conclude that “volume based expressions for the shape gradient often offer better accuracy than the use of formulas involving traces on boundaries”. In the present paper, the main focus is that it provides a compact yet efficient implementation for the level set method in topology optimization. We also show that the distributed shape derivative is useful to handle the ersatz material approach in level set-based structural optimization. Combining these techniques, we obtain a straightforward and general way of solving the shape optimization problem, from the rigorous theoretical computation of the shape derivative to the numerical implementation.

The choice of the software FEniCS for the implementation is motivated by the fact that it is easy to implement complicated variational formulations in FEniCS thanks to a near-mathematical notation, which is appropriate in our case since the expression of the distributed shape derivative is usually lengthy. The FEniCS Project is a collaborative project with a particular focus on automated solution of differential equations by finite element methods; see [6, 39].

The paper is structured as follows. In Section 2 we recall the definition of shape derivatives and how to compute them using the averaged adjoint method [36, 54]. In Section 3 we discuss the differences between boundary and domain expressions of the shape derivative. In Section 4 we compute the different expressions of the shape derivative, including for the ersatz material approach, and show how to compute descent directions. In section 5 we explain the level set method used in the present paper, which is a slight variation of the usual level set method suited for the distributed shape derivative. In this section we also describe the discretization and reinitialization procedures. In section 6 we explain in details the numerical implementation. In section 7 we show numerical results for the classical benchmarks. Finally, in section 8 we discuss the computation time and the influence of the initialization on the optimal design. In the appendix we also show the code for the main file `compliance.py`.

## 2. SHAPE DERIVATIVES

In this section we recall basic notions about the *shape derivative*, which is the main tool used in this paper, and an abstract result to compute it. Let  $\mathcal{P}(\mathcal{D})$  be the set of subsets of  $\mathcal{D} \subset \mathbb{R}^m$  compactly contained in  $\mathcal{D}$ , where the so-called *universe*  $\mathcal{D} \subset \mathbb{R}^m$  is assumed to be open and bounded. In our numerical application,  $\mathcal{D}$  is a rectangle. We define for  $k \geq 0$  and  $0 \leq \alpha \leq 1$ ,

$$C_c^{k,\alpha}(\mathcal{D}, \mathbb{R}^m) := \{\theta \in C^{k,\alpha}(\mathcal{D}, \mathbb{R}^m) \mid \theta \text{ has compact support in } \mathcal{D}\},$$

and  $C_c^k(\mathcal{D}, \mathbb{R}^m)$  in a similar way. Consider a vector field  $\theta \in C_c^{0,1}(\mathcal{D}, \mathbb{R}^m)$  and the associated flow  $T_t^\theta : \overline{\mathcal{D}} \rightarrow \mathbb{R}^m$ ,  $t \in [0, \tau]$  defined for each  $x_0 \in \overline{\mathcal{D}}$  as  $T_t^\theta(x_0) := x(t)$ , where  $x : [0, \tau] \rightarrow \mathbb{R}^m$  solves

$$(1) \quad \dot{x}(t) = \theta(x(t)) \quad \text{for } t \in [0, \tau], \quad x(0) = x_0.$$

We often use the simpler notation  $T_t = T_t^\theta$  when no confusion is possible. Let  $\Omega \in \mathcal{P}(\mathcal{D})$  and denote  $n$  the outward unit normal vector to  $\Omega$ . We consider the family of perturbed domains

$$(2) \quad \Omega_t := T_t^\theta(\Omega).$$

**Definition 1.** Let  $J : \mathbb{P} \rightarrow \mathbb{R}$  be a shape function defined on some admissible set  $\mathbb{P} \subset \mathcal{P}(\mathcal{D})$ .

(i) The Eulerian semiderivative of  $J$  at  $\Omega$  in direction  $\theta \in C_c^{0,1}(\mathcal{D}, \mathbb{R}^m)$ , when the limit exists, is defined by

$$(3) \quad dJ(\Omega; \theta) := \lim_{t \searrow 0} \frac{J(\Omega_t) - J(\Omega)}{t}.$$

(i)  $J$  is said to be shape differentiable at  $\Omega$  if it has a Eulerian semiderivative at  $\Omega$  for all  $\theta \in C_c^{0,1}(\mathcal{D}, \mathbb{R}^m)$  and the mapping

$$dJ(\Omega) : C_c^{0,1}(\mathcal{D}, \mathbb{R}^m) \rightarrow \mathbb{R}, \quad \theta \mapsto dJ(\Omega; \theta)$$

is linear and continuous, in which case  $dJ(\Omega)$  is called the shape derivative at  $\Omega$ .

- (ii) *The shape derivative  $dJ(\Omega)$  is of finite order if there is an integer  $l \geq 0$  and a constant  $c > 0$  such that for each compact  $K \subset \mathcal{D}$ ,*

$$|dJ(\Omega)(\theta)| \leq c\|\theta\|_l \quad \forall \theta \in C_c^\infty(K, \mathbb{R}^m),$$

where  $\|\theta\|_l := \sum_{|\alpha| \leq l} |D^\alpha \theta|_\infty$ . *The smallest such integer  $l \geq 0$  is called order of  $dJ(\Omega)$ .*

To compute the shape derivative of  $J(\Omega)$ , we use the averaged adjoint method, a Lagrangian-type method introduced in [54]; see also [36], and [20] for another Lagrangian method. Let two vector spaces  $\mathcal{E} = \mathcal{E}(\Omega)$ ,  $\mathcal{F} = \mathcal{F}(\Omega)$  and  $\tau > 0$  be given, and consider a parameterization  $\Omega_t = T_t(\Omega)$  for  $t \in [0, \tau]$ . Ultimately, our goal is to differentiate shape functions of the type  $J(\Omega_t)$  which can be written using a Lagrangian as  $J(\Omega_t) = \mathcal{L}(\Omega_t, u^t, \hat{\psi})$ , where  $u^t \in \mathcal{E}(\Omega_t)$  and  $\hat{\psi} \in \mathcal{F}(\Omega_t)$ .

The main appeal of the Lagrangian is that, to compute the derivative of  $J(\Omega_t)$ , we actually only need to compute the derivative with respect to  $t$  of

$$G(t, \varphi, \psi) := \mathcal{L}(T_t(\Omega), \varphi \circ T_t^{-1}, \psi \circ T_t^{-1}),$$

with  $G : [0, \tau] \times \mathcal{E} \times \mathcal{F} \rightarrow \mathbb{R}$  and to assign afterward the proper values to  $\varphi$  and  $\psi$ , which avoids to compute the derivative of  $u^t$  in  $\mathcal{L}(\Omega_t, u^t, \hat{\psi})$ ; see [54] for a detailed explanation.

In addition, in this paper we consider the following specific form

$$(4) \quad G(t, \varphi, \psi) := a(t, \varphi, \psi) + b(t, \varphi),$$

where

$$a : [0, \tau] \times \mathcal{E} \times \mathcal{F} \rightarrow \mathbb{R}, \quad b : [0, \tau] \times \mathcal{E} \rightarrow \mathbb{R},$$

are functions such that  $\psi \mapsto a(t, \varphi, \psi)$  is linear for all  $t \in [0, \tau]$  and  $\varphi \in \mathcal{E}$ . The function  $G$  is called *Lagrangian*. In the applications we have in mind, the function  $b$  arises from the objective function while  $a$  corresponds to the constraint, after transporting back to the fixed domain  $\Omega$ .

Let us assume that for each  $t \in [0, \tau]$  the equation

$$(5) \quad d_\psi G(t, u^t, 0; \hat{\psi}) = a(t, u^t, \hat{\psi}) = 0, \quad \text{for all } \hat{\psi} \in \mathcal{F},$$

admits a unique solution  $u^t \in \mathcal{E}$ , which is the case for the elasticity system we consider in this paper. Further, we make the following assumptions for  $G$ .

**Assumption (H0).** *For every  $(t, \psi) \in [0, \tau] \times \mathcal{F}$ ,*

- (i)  $[0, 1] \ni s \mapsto G(t, su^t + s(u^t - u^0), \psi)$  *is absolutely continuous,*
- (ii)  $[0, 1] \ni s \mapsto d_\varphi G(t, su^t + (1-s)u^0, \psi; \hat{\varphi})$  *belongs to  $L^1(0, 1)$  for all  $\hat{\varphi} \in \mathcal{E}$ .*

When Assumption (H0) is satisfied, for  $t \in [0, \tau]$  we introduce the *averaged adjoint equation* associated with  $u^t$  and  $u^0$ :

$$(6) \quad \text{Find } p^t \in \mathcal{F} \text{ such that } \int_0^1 d_\varphi G(t, su^t + (1-s)u^0, p^t; \hat{\varphi}) ds = 0 \quad \text{for all } \hat{\varphi} \in \mathcal{E}.$$

If  $\varphi \mapsto a(t, \varphi, \psi)$  is in addition linear, then (6) takes the simpler form

$$a(t, \hat{\varphi}, p^t) = - \int_0^1 d_\varphi b(t, su^t + (1-s)u^0; \hat{\varphi}) ds \quad \text{for all } \hat{\varphi} \in \mathcal{E}.$$

We can now state the main result of this section.

**Assumption (H1).** *We have*

$$\lim_{t \searrow 0} \frac{G(t, u^0, p^t) - G(0, u^0, p^0)}{t} = \partial_t G(0, u^0, p^0).$$

**Theorem 1.** *Let assumptions (H0) and (H1) be satisfied and assume there exists a unique solution  $p^t$  of the averaged adjoint equation (6). Then for  $\psi \in \mathcal{F}$  we obtain*

$$(7) \quad \frac{d}{dt} b(t, u^t)|_{t=0} = \frac{d}{dt} (G(t, u^t, \psi))|_{t=0} = \partial_t G(0, u^0, p^0).$$

Theorem 1 essentially says that to compute the derivative with respect to  $t$  of the cost functional  $b(t, u^t)$ , we only need to compute the partial derivative  $\partial_t G(0, u^0, p^0)$ , thus it is not necessary to compute the derivative of  $u^t$ .

### 3. REPRESENTATIONS OF THE SHAPE DERIVATIVE

The shape derivative from Definition 1 has a particular structure. Intuitively, it is clear that the form functional stays constant for a transformation  $\Phi$  that leaves  $\Omega$  unchanged, that is  $\Phi(\Omega) = \Omega$ , even if some points inside  $\Omega$  move, and consequently the shape derivative is zero in this case. This property is valid when  $\Omega$  is open or closed; cf. [20]. Another classical fact of shape optimization is that tangential perturbations of the boundary  $\partial\Omega$  produce a zero first-order shape derivative. These ideas lead to the following structure theorem proved by Zolésio.

**Theorem 2** (Structure Theorem). *Assume  $\partial\Omega$  is compact and  $J$  is shape differentiable. Assuming the shape derivative  $dJ(\Omega)$  is of order  $k \geq 0$  and  $\partial\Omega$  of class  $C^{k+1}$ , then there exists a linear and continuous functional  $g : C^k(\partial\Omega) \rightarrow \mathbb{R}$  such that for all  $\theta \in C_c^k(\mathcal{D}, \mathbb{R}^m)$ ,*

$$(8) \quad dJ(\Omega; \theta) = g(\theta|_{\partial\Omega} \cdot n).$$

*Proof.* See [20, pp. 480-481]. □

Sometimes it is preferable to write the shape derivative as a domain integral, the so-called distributed form, even if its support is on the boundary as shown by Theorem 2. The distributed form also has a particular tensor representation. We show a general relation between this tensor representation and the usual boundary expression of the shape derivative. The proofs for the results of this section can be found in [36].

**Definition 2.** *Let  $\Omega \in \mathbb{P}$  be a set with  $C^1$ -boundary. A shape differentiable function  $J$  of order 1 is said to admit a tensor representation if there exist tensors  $S_l \in L^1(\mathcal{D}, \mathcal{L}^l(\mathbb{R}^m, \mathbb{R}^m))$  and  $\mathfrak{S}_l \in L^1(\partial\Omega; \mathcal{L}^l(\mathbb{R}^m, \mathbb{R}^m))$ ,  $l = 0, 1$ , such that*

$$(9) \quad dJ(\Omega; \theta) = \int_{\mathcal{D}} S_1 \cdot D\theta + S_0 \cdot \theta \, dx + \int_{\partial\Omega} \mathfrak{S}_1 \cdot D_\Gamma \theta + \mathfrak{S}_0 \cdot \theta \, ds \quad \text{for all } \theta \in C_c^k(\mathcal{D}, \mathbb{R}^m),$$

where  $D_\Gamma \theta := D\theta - (D\theta n) \otimes n$  is the tangential derivative of  $\theta$  along  $\partial\Omega$ . Here  $\mathcal{L}^l(\mathbb{R}^m, \mathbb{R}^m)$  denotes the space of multilinear maps from  $(\mathbb{R}^m)^l$  to  $\mathbb{R}^m$ .

When  $\mathfrak{S}_1 = 0$  and  $\mathfrak{S}_0 = 0$ , we can reduce the regularity assumption on  $\Omega$ .

**Definition 3.** *Let  $\Omega \in \mathbb{P}$  be open. A shape differentiable function  $J$  of order 1 is said to admit a tensor representation if there exist tensors  $S_l \in L^1(\mathcal{D}, \mathcal{L}^l(\mathbb{R}^m, \mathbb{R}^m))$ ,  $l = 0, 1$ , such that*

$$(10) \quad dJ(\Omega; \theta) = \int_{\mathcal{D}} S_1 \cdot D\theta + S_0 \cdot \theta \, dx \quad \text{for all } \theta \in C_c^k(\mathcal{D}, \mathbb{R}^m).$$

In fact the tensor representation (9) can be defined for functionals of order  $k \geq 1$ , here we present only the case  $k = 1$  for simplicity; see [36] for the general case. Note that the tensor representations (9) and (10) are not unique. Each choice of tensors  $S_l$  and  $\mathfrak{S}_l$  leads to a different type of representation. In particular, an important case is when  $S_0 \equiv 0$ ,  $S_1 \equiv 0$ ,  $\mathfrak{S}_1 \equiv 0$  and  $\mathfrak{S}_0 = (\mathfrak{S}_0 \cdot n)n$  as this yields the *boundary expression* (8) from Theorem 2. When  $S_0$  or  $S_1$  are different from zero, we speak of *volume expression*, or *distributed form* of the shape derivative. The non-uniqueness of the tensor representation also means that the tensors in (9) or (10) are correlated. In Proposition 1 below, we describe these correlations, and we also describe the relations between the tensors from the boundary expression and from the volume expression of the shape derivative.

**Proposition 1.** *Let  $\Omega$  be a subset of  $\mathcal{D}$  with  $C^1$ -boundary. Suppose that the derivative  $dJ(\Omega)$  has the tensor representation (9). If  $S_l$ ,  $l = 0, 1$  is of class  $W^{1,1}$  in  $\Omega$  and  $\mathcal{D} \setminus \overline{\Omega}$ , then indicating by  $+$  and  $-$  the restrictions of the tensors to  $\Omega$  and  $\mathcal{D} \setminus \overline{\Omega}$ , respectively, we get*

$$(11) \quad \begin{aligned} -\operatorname{div}(S_1^+) + S_0^+ &= 0 & \text{in } \Omega, \\ -\operatorname{div}(S_1^-) + S_0^- &= 0 & \text{in } \mathcal{D} \setminus \overline{\Omega}. \end{aligned}$$

If  $\partial\Omega$  is  $C^2$  and  $\mathfrak{S}_1 \in W^{1,1}(\partial\Omega; \mathcal{L}^1(\mathbb{R}^m, \mathbb{R}^m))$ , then we obtain the so-called *boundary expression* of the shape derivative:

$$(12) \quad dJ(\Omega)(\theta) = \int_{\partial\Omega} g_1 \theta \cdot n \, ds,$$

where

$$(13) \quad g_1 := [(S_1^+ - S_1^-)n] \cdot n + \mathfrak{S}_0 \cdot n + \mathfrak{S}_1 \cdot D_\Gamma n - \operatorname{div}_\Gamma(\mathfrak{S}_1^T n) + \mathcal{H}(\mathfrak{S}_1^T n \cdot n).$$

and  $\mathcal{H} = \operatorname{div}_\Gamma n$  denotes the mean curvature of  $\partial\Omega$  while  $\operatorname{div}_\Gamma := \operatorname{tr}(D_\Gamma)$  is the tangential divergence.

*Proof.* See [36]. □

Using the averaged adjoint approach from Theorem 1 yields the tensor representations (9) or (10) of the shape derivative. Then Proposition 1 can be used to derive the standard boundary expression (12) of the shape gradient from the tensor representation (9) if  $\Omega$  has enough regularity.

In order to emphasize the differences between the distributed and the boundary expression of the shape derivative, we will denote the distributed expression (9) or (10) by  $dJ^{\text{vol}}(\Omega; \theta)$ , when  $S_0$  or  $S_1$  are different from zero, and the boundary expression (12) by  $dJ^{\text{surf}}(\Omega; \theta)$ . Note that if the domain is  $C^2$ , Proposition 1 shows that

$$dJ^{\text{vol}}(\Omega; \theta) = dJ^{\text{surf}}(\Omega; \theta).$$

If  $\Omega$  is less regular than  $C^2$ , it may happen that  $dJ^{\text{surf}}(\Omega; \theta)$  does not exist. Note that even in this case, Theorem 2 is valid, which means that  $dJ^{\text{vol}}(\Omega; \theta)$  is a distribution on the boundary, even if written as a domain integral.

#### 4. SHAPE DERIVATIVE OF THE COMPLIANCE

In this section we apply the general results of the previous sections to the particular case of linearized elasticity. Let  $\Omega \subset \mathcal{D} \subset \mathbb{R}^m$ ,  $m = 2, 3$ . Its boundary  $\partial\Omega$  is decomposed in three complementary parts  $\Gamma_d$ ,  $\Gamma_n$  and  $\Gamma$ , and a homogeneous Dirichlet (respectively Neumann) boundary condition is imposed on  $\Gamma_d$  (resp.  $\Gamma_n$ ). The free boundary is  $\Gamma$ , where a homogeneous Neumann condition is imposed. Let  $H_d^1(\Omega)^m$  be the space of vector fields in  $H^1(\Omega)^m$  which satisfy the homogeneous Dirichlet boundary conditions on  $\Gamma_d$ . Let  $g \in H^{-1/2}(\Gamma_n)^m$  be a given surface load.

We consider the elasticity system

$$(14) \quad -\operatorname{div} Ae(u) = 0 \text{ in } \Omega,$$

$$(15) \quad u = 0 \text{ on } \Gamma_d,$$

$$(16) \quad Ae(u)n = g \text{ on } \Gamma_n,$$

$$(17) \quad Ae(u)n = 0 \text{ on } \Gamma.$$

The Hooke elasticity tensor  $A$  is defined by

$$A\xi = 2\mu\xi + \lambda \operatorname{tr}(\xi)I_d,$$

where  $\xi \in \mathbb{R}^{m \times m}$ ,  $\mu, \lambda$  are the Lamé parameters and  $I_d$  is the identity matrix. Also, the symmetrized gradient is

$$e(u) = (Du + Du^\top)/2,$$

where  $Du^\top$  denotes the transpose of  $Du$ . The variational formulation of (14)-(17) is:

$$\text{find } u \in H_d^1(\Omega)^m \text{ such that } \int_{\Omega} Ae(u) \cdot e(v) = \int_{\Gamma_n} g \cdot v \text{ for all } v \in H_d^1(\Omega)^m.$$

We introduce the compliance of the system, as a shape function of the set  $\Omega$ :

$$J(\Omega) := \int_{\Gamma_n} g \cdot u = - \int_{\Omega} Ae(u) \cdot e(u) + 2 \int_{\Gamma_n} g \cdot u = \int_{\Omega} Ae(u) \cdot e(u).$$

**4.1. Boundary and distributed shape derivative.** We compute here the distributed expression  $dJ^{\text{vol}}(\Omega; \theta)$  and the boundary expression  $dJ^{\text{surf}}(\Omega; \theta)$  of the shape derivative of  $J(\Omega)$ . Some of the following results are standard, see for instance [5, 20, 42, 53], however we reproduce them here mainly to emphasize and discuss the relations between the distributed and the boundary expressions of the shape derivative, and also to provide a self-contained presentation. The presentation is also useful as it shows a general procedure, based on the averaged adjoint method, which can be applied for various other cost functionals and partial differential equations, including nonlinear ones; see [29].

We introduce a parameterized domain  $\Omega_t = T_t^\theta(\Omega)$  as in (2), such that  $T_t^\theta(\Gamma_n) = \Gamma_n$ , i.e.  $\Gamma_n$  is fixed during the optimization process. We denote  $u_t$  the solution in the domain  $\Omega_t$ . Note that due to the chain rule we have the relation

$$(18) \quad D(u_t \circ T_t) = (Du_t \circ T_t)DT_t.$$

Also, defining  $u^t := u_t \circ T_t$ , we introduce the notation

$$(19) \quad E(t, u^t) := e(u_t) \circ T_t = (Du^t DT_t^{-1} + DT_t^{-\top}(Du^t)^\top)/2,$$

where  $M^\top$  is the transpose of a matrix  $M$ . The variational formulation of the PDE in  $\Omega_t$  is

$$(20) \quad \text{Find } u_t \in H_d^1(\Omega_t)^m \text{ such that } \int_{\Omega_t} Ae(u_t) \cdot e(v_t) = \int_{\Gamma_n} g \cdot v_t \quad \text{for all } v_t \in H_d^1(\Omega_t)^m.$$

We proceed with the change of variable  $y = T_t(x)$  in (20) which yields

$$(21) \quad \int_{\Omega} Ae(u_t) \circ T_t \cdot e(v_t) \circ T_t \xi(t) = \int_{\Gamma_n} g \cdot v_t \circ T_t \quad \text{for all } v_t \in H_d^1(\Omega_t)^m,$$

where  $\xi(t) := |\det DT_t|$  is the Jacobian of the transformation  $y = T_t(x)$ . Note that the Jacobian does not appear in the integral on  $\Gamma_n$ , since  $T_t(\Gamma_n) = \Gamma_n$ . In view of (19), we can rewrite (21) as

$$(22) \quad \int_{\Omega} AE(t, u^t) \cdot E(t, v) \xi(t) = \int_{\Gamma_n} g \cdot v \quad \text{for all } v \in H_d^1(\Omega)^m.$$

In a similar way, we have, using the same change of variable,

$$(23) \quad J(\Omega_t) = \int_{\Omega_t} Ae(u_t) \cdot e(u_t) = \int_{\Omega} AE(t, u^t) \cdot E(t, u^t) \xi(t).$$

In view of (22) and (23), our objective is to apply Theorem 1 with  $\mathcal{E} = \mathcal{F} = H_d^1(\Omega)^m$  and the Lagrangian

$$G(t, \varphi, \psi) := \int_{\Omega} AE(t, \varphi) \cdot E(t, \varphi) \xi(t) + \int_{\Omega} AE(t, \varphi) \cdot E(t, \psi) \xi(t) - \int_{\Gamma_n} g \cdot \psi.$$

The adjoint is given as the solution of the following first-order optimality condition

$$\partial_{\varphi} G(0, u, p)(\hat{\varphi}) = 0 \text{ for all } \hat{\varphi} \in H_d^1(\Omega)^m,$$

which yields using  $A = A^T$ ,

$$2 \int_{\Omega} AE(0, u) \cdot E(0, \hat{\varphi}) + \int_{\Omega} AE(0, \hat{\varphi}) \cdot E(0, p) = 0 \text{ for all } \hat{\varphi} \in H_d^1(\Omega)^m.$$

Since  $E(0, v) = e(v)$  for  $v \in H_d^1(\Omega)^m$  and  $A = A^T$  we get

$$\int_{\Omega} Ae(p) \cdot e(\hat{\varphi}) = -2 \int_{\Omega} Ae(u) \cdot e(\hat{\varphi}) \text{ for all } \hat{\varphi} \in H_d^1(\Omega)^m.$$

This shows that  $p = -2u$ .

Next we can apply Theorem 1 to compute the shape derivative. Here we do not write the verification of the assumptions required to apply Theorem 1 as this is not the purpose of this paper to go into these details. Instead, we refer to [29, 36] for a detailed verification of the assumptions for similar problems, which can easily be extrapolated for the present problem. Assuming that the assumptions of Theorem 1 are satisfied, we obtain the shape derivative

$$dJ(\Omega; \theta) = \frac{d}{dt}(G(t, u^t, \psi))|_{t=0} = \partial_t G(0, u, p),$$

which yields

$$\begin{aligned} dJ(\Omega; \theta) &= \int_{\Omega} A \partial_t E(0, u) \cdot E(0, u) + AE(0, u) \cdot \partial_t E(0, u) + AE(0, u) \cdot E(0, u) \operatorname{div} \theta \\ &\quad + \int_{\Omega} A \partial_t E(0, u) \cdot E(0, p) + AE(0, u) \cdot \partial_t E(0, p) + AE(0, u) \cdot E(0, p) \operatorname{div} \theta. \end{aligned}$$

We also compute, using  $E(0, v) = e(v)$  for  $v \in H_d^1(\Omega)^m$ ,

$$\partial_t E(0, v) = (-Dv D\theta - D\theta^T Dv^T)/2.$$

Using the property  $A = A^T$  and  $(Ae(v))^T = Ae(v)$  we obtain

$$\begin{aligned} dJ(\Omega; \theta) &= - \int_{\Omega} \frac{1}{2} (Du^T Ae(p) + Du^T (Ae(p))^T) \cdot D\theta \\ &\quad - \int_{\Omega} \frac{1}{2} (Dp^T Ae(u) + Dp^T (Ae(u))^T) \cdot D\theta + \int_{\Omega} Ae(u) \cdot e(p) \operatorname{div} \theta \\ &\quad - \int_{\Omega} (Du^T Ae(u) + Du^T (Ae(u))^T) \cdot D\theta + \int_{\Omega} Ae(u) \cdot e(u) \operatorname{div} \theta \\ &= - \int_{\Omega} Du^T Ae(p) \cdot D\theta - \int_{\Omega} Dp^T Ae(u) \cdot D\theta + \int_{\Omega} Ae(u) \cdot e(p) \operatorname{div} \theta \\ &\quad - \int_{\Omega} 2Du^T Ae(u) \cdot D\theta + \int_{\Omega} Ae(u) \cdot e(u) \operatorname{div} \theta. \end{aligned}$$

Using  $p = -2u$  obtained above, we get the following volume expression of the shape derivative

$$dJ(\Omega; \theta) = \int_{\Omega} 2Du^T Ae(u) \cdot D\theta - Ae(u) \cdot e(u) \operatorname{div} \theta.$$

Finally, we would like to express this distributed shape derivative in the tensor form (10). This is easily done using vector calculus and we get:

$$(24) \quad dJ^{\text{vol}}(\Omega; \theta) = \int_{\Omega} S_1 \cdot D\theta,$$

with

$$(25) \quad S_1 := 2Du^T Ae(u) - Ae(u) \cdot e(u) I_d \quad \text{in } \Omega.$$

A similar formula can be found in [42, Section 2.5], for a slightly different case, and where  $S_1$  is identified as the energy-momentum tensor in continuum mechanics introduced by Eshelby in [23]. Compare also (24)-(25) with the shape derivative in [55, Theorem 3.3], also in the framework of linearized elasticity but for a different functional. Formula (24) is convenient for the numerics as we will see that it can be implemented in a straightforward way in FEniCS.

Now, assuming  $\Omega$  is  $C^2$  and using (24) and (12),(13) of Proposition 1, we obtain the boundary expression of the shape derivative

$$dJ^{\text{surf}}(\Omega; \theta) = \int_{\partial\Omega} (S_1 n \cdot n) \theta \cdot n = \int_{\Gamma \cup \Gamma_d} (S_1 n \cdot n) \theta \cdot n,$$

since  $\Gamma_n$  is fixed and  $\mathfrak{S}_0 \equiv 0$ ,  $\mathfrak{S}_1 \equiv 0$  in (13). Then we compute

$$S_1 n \cdot n = 2Du^T Ae(u) n \cdot n - Ae(u) \cdot e(u) = 2Ae(u) n \cdot Dun - Ae(u) \cdot e(u).$$

On  $\Gamma$ , we have  $Ae(u) n = 0$  which yields

$$S_1 n \cdot n = -Ae(u) \cdot e(u) \text{ on } \Gamma.$$

On  $\Gamma_d$ , we have  $u = 0$  and consequently  $D_\Gamma u := Du - (Dun) \otimes n = 0$ . Thus we compute

$$Ae(u) \cdot Du = Ae(u) \cdot ((Dun) \otimes n) = Ae(u) n \cdot Dun.$$

Using  $(Ae(u))^T = Ae(u)$  we also have  $Ae(u) \cdot e(u) = Ae(u) \cdot Du$  so these results yield

$$S_1 n \cdot n = Ae(u) \cdot e(u) \text{ on } \Gamma_d,$$

which yields the usual formula

$$(26) \quad dJ^{\text{surf}}(\Omega; \theta) = \int_{\Gamma} -Ae(u) \cdot e(u) \theta \cdot n + \int_{\Gamma_d} Ae(u) \cdot e(u) \theta \cdot n,$$

compare for instance with the formula in [5, Theorem 7].

**4.2. The ersatz material case.** The ersatz material approach is commonly used in level set-based topology optimization of structures; see for instance [5, 63]. It is convenient as it allows to work on a fixed domain  $\mathcal{D}$  instead of the moving domain  $\Omega$ , but also can create instability issues as pointed out in [18]. The idea of the ersatz material method is that a fixed domain  $\mathcal{D}$  is filled with two homogeneous materials with different Hooke elasticity tensors  $A_0$  and  $A_1$  defined by

$$A_i \xi = 2\mu_i \xi + \lambda_i (\operatorname{Tr} \xi) I_d, \quad i = 0, 1.$$

with Lamé moduli  $\lambda_i$  and  $\mu_i$  for  $i = 0, 1$ ,  $I_d$  is the identity operator and  $\xi$  is a matrix. The first material lays in the open subset  $\Omega$  of  $\mathcal{D}$  and the background material fills the complement so that Hooke's law is written in  $\mathcal{D}$  as

$$(27) \quad A_\Omega = A_0 \chi_\Omega + \epsilon A_0 \chi_{\mathcal{D} \setminus \Omega},$$

where  $\chi_\Omega$  denotes the indicator function of  $\Omega$ , and  $\epsilon$  is a given small parameter. Hence the region  $\mathcal{D} \setminus \Omega$  represents a “weak phase” whereas  $\Omega$  is the “strong phase”. The optimization is still performed with respect to the variable set  $\Omega$ , but here  $\Omega$  is embedded in a fixed, larger set  $\mathcal{D}$ . In our numerics for instance,  $\mathcal{D}$  is a fixed rectangle.

Often the shape derivative (26), which corresponds to the problem without ersatz material, is used for the optimization, but the elasticity system is solved using the ersatz material, so there is a mismatch. This mismatch is small, since the tensor of the ersatz material has a small amplitude, which justifies the approach. The reason why this mismatch is tolerated in the numerics is probably because the boundary expression of the shape derivative in that case is impractical to handle numerically, as it requires to compute the jump of the gradient across the moving interface between the strong and the weak phases; see (34).

In any case, it is more precise to use the proper shape derivative corresponding to the ersatz material framework for the numerics, in order to avoid this mismatch. Another advantage of using the exact formula for the ersatz

approach is that this formula is actually valid for any value of  $\epsilon$ , and not only for  $\epsilon$  small. This can be used for a mixture of two materials for instance. We show here that computing and implementing the formula of the distributed shape derivative is not more difficult for the ersatz material approach, therefore we use this formula in the numerics instead of (24) or (26).

In the ersatz material approach, the displacement field  $u \in H_d^1(\Omega)^m$  is the solution of the linearized elasticity system

$$(28) \quad -\operatorname{div} A_\Omega e(u) = 0 \text{ in } \mathcal{D},$$

$$(29) \quad u = 0 \text{ on } \Gamma_d,$$

$$(30) \quad A_\Omega e(u)n = g \text{ on } \Gamma_n,$$

$$(31) \quad A_\Omega e(u)n = 0 \text{ on } \Gamma,$$

where  $g \in H^{-1/2}(\Gamma_n)^m$  is a given surface load. Note that in (28)-(31) the definitions of  $\Gamma_n$ ,  $\Gamma_d$  and  $\Gamma$  are different from Section 4, indeed we have now  $\partial\mathcal{D} = \Gamma_n \cup \Gamma \cup \Gamma_d$ , so that  $\Gamma_n$ ,  $\Gamma_d$  and  $\Gamma$  are fixed, and the free boundary is now the interface  $\partial\Omega \subset \mathcal{D}$ .

In the case of the ersatz material the compliance is given by

$$J(\Omega) := \int_{\Gamma_n} g \cdot u = - \int_{\mathcal{D}} A_\Omega e(u) \cdot e(u) + 2 \int_{\Gamma_n} g \cdot u = \int_{\mathcal{D}} A_\Omega e(u) \cdot e(u).$$

To compute the shape derivative, the calculation is exactly the same as in Section 4, except that one needs to write  $J(\Omega)$  as the sum of two integrals, one on  $\Omega$  and the other on  $\mathcal{D} \setminus \Omega$ , due to the jump in  $A_\Omega$  across the interface  $\partial\Omega$ . This yields eventually

$$(32) \quad dJ^{\text{vol}}(\Omega; \theta) = \int_{\mathcal{D}} S_1 \cdot D\theta,$$

with

$$(33) \quad S_1 = 2Du^\top A_\Omega e(u) - A_\Omega e(u) \cdot e(u)I_d \quad \text{in } \mathcal{D}.$$

Note that (33) is similar to (25), the main difference being that (33) is defined in  $\mathcal{D}$  and (25) is defined in  $\Omega$ . Thus from a numerical point of view, (33) is not more difficult to compute than (25).

Applying Proposition 1 with  $\mathfrak{S}_0 = 0$  and  $\mathfrak{S}_1 = 0$ , assuming  $\theta = 0$  on  $\partial\mathcal{D}$  and  $\partial\Omega$  is  $C^2$ , we obtain the boundary expression

$$dJ^{\text{surf}}(\Omega; \theta) = \int_{\partial\Omega} [(S_1^+ - S_1^-)n] \cdot n \theta \cdot n,$$

with

$$[(S_1^+ - S_1^-)n] \cdot n = -\llbracket Ae(u) \cdot e(u) \rrbracket + 2A_0e(u)^+ n \cdot Du^+ n - 2\epsilon A_0e(u)^- n \cdot Du^- n,$$

and where the exponents  $(\cdot)^+$  and  $(\cdot)^-$  denote the restrictions to  $\Omega$  and  $\mathcal{D} \setminus \Omega$ , respectively. Also

$$\llbracket v \rrbracket := \gamma_\Omega(v) - \gamma_{\mathcal{D} \setminus \Omega}(v)$$

denotes the jump of a function  $v$  across the interface  $\partial\Omega$ ; here  $\gamma_\Omega(v)$  is the trace of  $v|_\Omega$  on  $\partial\Omega$ . Using the transmission condition

$$A_0e(u)^+ n = \epsilon A_0e(u)^- n \text{ on } \partial\Omega,$$

we obtain

$$(34) \quad dJ^{\text{surf}}(\Omega; \theta) = \int_{\partial\Omega} (2\epsilon A_0e(u^-)n \cdot \llbracket Du \rrbracket n - \llbracket Ae(u) \cdot e(u) \rrbracket) \theta \cdot n.$$

In order to compare formulae (34) and (26), one needs to keep in mind that here  $\Gamma_d$  is fixed, therefore, unlike in (26), there is no term on  $\Gamma_d$  in (34). The other two main differences between (34) and (26) are the small perturbation term

$$(2\epsilon A_0e(u^-)n \cdot \llbracket Dun \rrbracket$$

and the fact that  $\llbracket Ae(u) \cdot e(u) \rrbracket$  is a jump across the interface  $\partial\Omega$ .



**4.3. Descent direction.** For our gradient method we are looking for a descent direction  $\theta$ , i.e. a vector field satisfying

$$dJ(\Omega; \theta) < 0.$$

When  $dJ(\Omega; \theta)$  is written using the boundary expression

$$dJ^{\text{surf}}(\Omega; \theta) = \int_{\partial\Omega} G(\Omega) \theta \cdot n,$$

then a simple choice is to take  $\theta = -G(\Omega) \cdot n$ . However, this choice assumes that  $G(\Omega)$  and  $\partial\Omega$  are quite regular, and in practice this may yield a  $\theta$  with a poor regularity and lead to an unstable behaviour of the algorithm such as irregular or oscillating boundaries. A better choice is to find a smoother descent direction by solving:

$$(35) \quad \text{find } \theta \in \mathbb{H}(\partial\Omega) \text{ such that } \mathcal{B}(\theta, \xi) = -dJ^{\text{surf}}(\Omega; \xi) \text{ for all } \xi \in \mathbb{H}(\partial\Omega),$$

where  $\mathbb{H}(\partial\Omega)$  is an appropriate Sobolev space of vector fields on  $\partial\Omega$  and  $\mathcal{B} : \mathbb{H}(\partial\Omega) \times \mathbb{H}(\partial\Omega) \rightarrow \mathbb{R}$ ,  $k \geq 1$ , is a positive definite bilinear form on  $\partial\Omega$ .

In the case of the present paper we use the distributed expression of the shape derivative (24) and (32), therefore we use a positive definite bilinear form  $\mathcal{B} : \mathbb{H}(\mathcal{D}) \times \mathbb{H}(\mathcal{D}) \rightarrow \mathbb{R}$ , where  $\mathbb{H}(\mathcal{D})$  is an appropriate Sobolev space of vector fields on  $\mathcal{D}$ :

$$(36) \quad \text{find } \theta \in \mathbb{H}(\mathcal{D}) \text{ such that } \mathcal{B}(\theta, \xi) = -dJ^{\text{vol}}(\Omega; \xi) \text{ for all } \xi \in \mathbb{H}(\mathcal{D}),$$

With this choice, the solution  $\theta$  of (36) is defined on all of  $\mathcal{D}$  and is a descent direction since  $dJ(\Omega; \theta) = -\mathcal{B}(\theta, \theta) < 0$  if  $\theta \neq 0$ .

It is also possible to merge the two approaches by substituting  $dJ^{\text{vol}}(\Omega; \theta)$  with  $dJ^{\text{surf}}(\Omega; \theta)$  in (36). This was done in [19] where a strong improvement of the rate of convergence of the level-set method was observed. In our algorithm we choose  $\mathbb{H}(\mathcal{D}) = H^1(\mathcal{D})^m$  and

$$(37) \quad \mathcal{B}(\theta, \xi) = \int_{\mathcal{D}} \alpha_1 D\theta \cdot D\xi + \alpha_2 \theta \cdot \xi,$$

with  $\alpha_1 = 1$  and  $\alpha_0 = 0.1$ . We also take the boundary conditions  $\theta \cdot n = 0$  on  $\partial\mathcal{D}$ ; see the discussion in Section 6.5 for details.

## 5. LEVEL SET METHOD

The level set method, originally introduced in [44], gives a general framework for the computation of evolving interfaces using an implicit representation of these interfaces. The core idea of this method is to represent the boundary of the moving domain  $\Omega_t \subset \mathcal{D} \in \mathbb{R}^N$  as the level set of a continuous function  $\phi(\cdot, t) : \mathcal{D} \rightarrow \mathbb{R}$ .

Let us consider the family of domains  $\Omega_t \subset \mathcal{D}$  as defined in (2). Each domain  $\Omega_t$  can be defined as

$$(38) \quad \Omega_t := \{x \in \mathcal{D}, \phi(x, t) < 0\},$$

where  $\phi : \mathcal{D} \times \mathbb{R}^+ \rightarrow \mathbb{R}$  is continuous and called *level set function*. Indeed, if we assume  $|\nabla\phi(\cdot, t)| \neq 0$  on the set  $\{x \in \mathcal{D}, \phi(x, t) = 0\}$  then we have

$$(39) \quad \partial\Omega_t = \{x \in \mathcal{D}, \phi(x, t) = 0\},$$

i.e. the boundary  $\partial\Omega_t$  is the zero level set of  $\phi(\cdot, t)$ .

Let  $x(t)$  be the position of a moving boundary point of  $\partial\Omega_t$ , with velocity  $\dot{x}(t) = \theta(x(t))$  according to (1). Differentiating the relation  $\phi(x(t), t) = 0$  with respect to  $t$  yields the Hamilton-Jacobi equation:

$$\partial_t \phi(x(t), t) + \theta(x(t)) \cdot \nabla \phi(x(t), t) = 0 \quad \text{in } \partial\Omega_t \times \mathbb{R}^+,$$

which is then extended to all of  $\mathcal{D}$  via the equation

$$(40) \quad \partial_t \phi(x, t) + \theta(x) \cdot \nabla \phi(x, t) = 0 \quad \text{in } \mathcal{D} \times \mathbb{R}^+,$$

or alternatively to  $U \times \mathbb{R}^+$  where  $U$  is a neighbourhood of  $\partial\Omega_t$ .

Originally, the level set method has been designed to track smooth interfaces moving along the normal direction to the boundary. Theoretically, this is supported by Theorem 2, i.e. if the domain  $\Omega_t$  and the shape gradient are smooth enough then the shape derivative only depends on  $\theta \cdot n$  on  $\partial\Omega_t$ . In this case, we may choose for the evolution a vector field  $\theta = \vartheta_n n$  on  $\partial\Omega_t$ . Then, noting that an extension to  $\mathcal{D}$  of the unit outward normal vector  $n$  to  $\Omega_t$  is given by  $n = \nabla\phi/|\nabla\phi|$ , and extending  $\vartheta_n$  to all of  $\mathcal{D}$ , one obtains from (40) the level set equation

$$(41) \quad \partial_t \phi + \vartheta_n |\nabla\phi| = 0 \quad \text{in } \mathcal{D} \times \mathbb{R}^+.$$

The initial data  $\phi(x, 0) = \phi_0(x)$  accompanying the Hamilton-Jacobi equation (40) or (41) can be chosen as the signed distance function to the initial boundary  $\partial\Omega(0)$  in order to satisfy the condition  $|\nabla u| \neq 0$  on  $\partial\Omega$ , i.e.

$$(42) \quad \phi_0(x) = \begin{cases} d(x, \partial\Omega(0)), & \text{if } x \in (\Omega(0))^c, \\ -d(x, \partial\Omega(0)), & \text{if } x \in \Omega(0). \end{cases}$$

**5.1. Level set method and volume expression of the shape derivative.** In the case of the distributed shape derivative  $dJ^{\text{vol}}(\Omega; \theta)$  in (24) and (32),  $\phi$  is not governed by (41) but rather by the Hamilton-Jacobi equation (40). Indeed, we obtain a descent direction  $\theta$  defined in  $\mathcal{D}$  by solving (36), where  $dJ^{\text{vol}}(\Omega; \theta)$  is given by (24) or (32), which can subsequently be used in (40) to compute the evolution of  $\phi$ . On the other hand, in the usual level set method, one solves a PDE *on the boundary*  $\partial\Omega$  in an analogous way as for (36) (for instance using a Laplace-Beltrami operator), and uses the boundary expression (26) or (34) to obtain  $\vartheta_n = \theta \cdot n$  on  $\partial\Omega$ .

Numerically it is actually more straightforward in many cases to use (40) instead of (41). Indeed, when using (41),  $\vartheta_n$  is initially only given on  $\partial\Omega_t$  and must be extended to the entire domain  $\mathcal{D}$  or at least to a narrow band around  $\partial\Omega_t$ . Therefore it is convenient to use (40) with  $\theta$  already defined in  $\mathcal{D}$  as is the case of the distributed shape derivative, which provides an extension to  $\mathcal{D}$  or to a narrow band around  $\partial\Omega_t$ .

In shape optimization,  $\vartheta_n$  usually depends on the solution of one or several PDEs and their gradient. Since the boundary  $\partial\Omega_t$  in general does not match the grid nodes where  $\phi$  and the solutions of the partial differential equations are defined in the numerical application, the computation of  $\vartheta_n$  requires the interpolation on  $\partial\Omega_t$  of functions defined at the grid points only, complicating the numerical implementation and introducing an additional interpolation error. This is an issue in particular for interface problems, such as the problem of elasticity with ersatz material studied in this paper, where  $\vartheta_n$  is the jump of a function across the interface, as in (34), which requires multiple interpolations and is error-prone. In the distributed shape derivative framework  $\theta$  only needs to be defined at grid nodes.

**5.2. Discretization of the Hamilton-Jacobi equation.** Let  $\mathcal{D}$  be the unit square  $\mathcal{D} = (0, 1) \times (0, 1)$  to fix ideas. For the discretization of the Hamilton-Jacobi equation (40), we first define the mesh grid corresponding to  $\mathcal{D}$ . We introduce the nodes  $P_{ij}$  whose coordinates are given by  $(i\Delta x, j\Delta y)$ ,  $1 \leq i, j \leq N$  where  $\Delta x$  and  $\Delta y$  are the steps discretization in the  $x$  and  $y$  directions respectively. Let us also write  $t^k = k\Delta t$  the discrete time for  $k \in \mathbb{N}$ , where  $\Delta t$  is the time step. We are seeking for an approximation  $\phi_{ij}^k \simeq \phi(P_{ij}, t^k)$ .

In the usual level set method, the level set equation (41) is discretized using an explicit upwind scheme proposed by Osher and Sethian [43, 44, 50]. This scheme applies to the specific form (41) but is not suited to discretize (40) required for our application. Equation (40) is of the form

$$(43) \quad \partial_t \phi + H(\nabla \phi) = 0 \quad \text{in } \mathcal{D} \times \mathbb{R}^+,$$

where  $H(\nabla \phi) := \theta \cdot \nabla \phi$  is the so-called Hamiltonian. We use the Local Lax-Friedrichs flux originally conceived in [45] and which reduces in our case to:

$$\hat{H}^{LLF}(p^-, p^+, q^-, q^+) = H\left(\frac{p^- + p^+}{2}, \frac{q^- + q^+}{2}\right) - \frac{1}{2}(p^+ - p^-)\alpha^x - \frac{1}{2}(p^+ - p^-)\alpha^y,$$

where  $\alpha^x = |\theta_x|$ ,  $\alpha^y = |\theta_y|$ ,  $\theta = (\theta_x, \theta_y)$  and

$$\begin{aligned} p^- &= D_x^- \phi_{ij} = \frac{\phi_{ij} - \phi_{i-1,j}}{\Delta x}, & p^+ &= D_x^+ \phi_{ij} = \frac{\phi_{i+1,j} - \phi_{ij}}{\Delta x}, \\ q^- &= D_y^- \phi_{ij} = \frac{\phi_{ij} - \phi_{i,j-1}}{\Delta y}, & q^+ &= D_y^+ \phi_{ij} = \frac{\phi_{i,j+1} - \phi_{ij}}{\Delta y} \end{aligned}$$

are the backward and forward approximations of the  $x$ -derivative and  $y$ -derivative of  $\phi$  at  $P_{ij}$ , respectively. Using a forward Euler time discretization, the numerical scheme corresponding to (40) is

$$(44) \quad \phi_{ij}^{k+1} = \phi_{ij}^k - \Delta t \hat{H}^{LLF}(p^-, p^+, q^-, q^+)$$

where  $p^-, p^+, q^-, q^+$  are computed for  $\phi_{ij}^k$ .

The computational efficiency of the level set method could be improved by using the so-called *narrow band* approach introduced in [2], which consists in computing and updating the level set function only on a thin region around the interface. This allows to reduce the complexity of the problem to  $N \log(N)$  instead of  $N^2$  in two dimensions. In this paper we do not implement this approach to keep the code simple and compact, but we mention that it could also be applied to the distributed shape derivative approach and equation (40) by taking  $\theta$  with a support in a narrow band around the moving interface, which can be achieved by choosing a smaller space in (36).

**5.3. Reinitialization.** For numerical accuracy, the solution of the level set equation (40) should not be too flat or too steep. This is fulfilled for instance if  $\phi$  is the distance function i.e.  $|\nabla\phi| = 1$ . Even if one initializes  $\phi$  using a signed distance function, the solution  $\phi$  of the level set equation (40) does not generally remain close to a distance function. We occasionally perform a reinitialization of  $\phi$  by solving a parabolic equation up to the stationary state as in [47]; see also [25, 26].

We rewrite here briefly the procedure for the reinitialization for the convenience of the reader. The reinitialization is performed by solving, up to the stationary state

$$\begin{aligned}\varphi_\tau + S(\phi)(|\nabla\varphi| - 1) &= 0 \text{ in } \mathcal{D} \times \mathbb{R}^+, \\ \varphi(x, 0) &= \phi(x, t), \quad x \in \mathcal{D},\end{aligned}$$

where  $S(\phi)$  is an approximation of the sign function

$$(45) \quad S(\phi) = \frac{\phi}{\sqrt{\phi^2 + |\nabla\phi|^2 \epsilon^2}},$$

with  $\epsilon = \min(\Delta x, \Delta y)$ , where  $\Delta x$  and  $\Delta y$  stand for the space discretization steps in the  $x$  and  $y$  directions, respectively.

For the discretization we use the standard explicit upwind scheme from (Osher and Fedkiw, 2004; Osher and Sethian, 1988; Sethian, 1996).

$$(46) \quad \varphi_{ij}^{k+1} = \varphi_{ij}^k - \Delta t G(p^-, p^+, q^-, q^+),$$

where

$$(47) \quad G(p^-, p^+, q^-, q^+) = \max(S(\phi_{ij}), 0)G^+ + \min(S(\phi_{ij}), 0)G^-,$$

and

$$(48) \quad G^+ = [\max(p^-, 0)^2 + \min(p^+, 0)^2 + \max(q^-, 0)^2 + \min(q^+, 0)^2]^{1/2},$$

$$(49) \quad G^- = [\min(p^-, 0)^2 + \max(p^+, 0)^2 + \min(q^-, 0)^2 + \max(q^+, 0)^2]^{1/2},$$

and where  $p^-, p^+, q^-, q^+$  are computed for  $\phi_{ij}^k$ .

## 6. NUMERICAL IMPLEMENTATION

In this section we explain the implementation step by step. The code presented in this paper has been written using FEniCS 2016.2, which can be downloaded at <https://fenicsproject.org/>. With a small number of modifications, the code may also run with earlier versions of FEniCS.

The code can be downloaded at [http://antoinelaurain.com/recherche\\_struct\\_eng.htm](http://antoinelaurain.com/recherche_struct_eng.htm) and is intended for educational purpose.

For the numerical problem we consider an additional volume constraint, so the functional that we minimize is

$$J(\Omega) + \Lambda \mathcal{V}(\Omega),$$

where  $\Lambda$  is a constant and  $\mathcal{V}(\Omega) = |\Omega|$  is the volume of  $\Omega$ . It is known that the distributed shape derivative of  $\mathcal{V}(\Omega)$  is given by

$$d\mathcal{V}^{\text{vol}}(\Omega; \theta) = \int_{\Omega} \text{div}(\theta).$$

The code consists of two files. The main file is `compliance.py` which can be found in the appendix. The file `init.py` is used to initialize the data which depends on the chosen case. The user can choose between the six following cases: `cantilever`, `cantilever_asyymmetric`, `half_wheel`, `bridge`, `MBB_beam`, and `cantilever_twoforces`. For instance, to run the cantilever case, the command line is

```
python compliance.py cantilever
```

In the first few lines of the code, we import the modules `dolfin`, `init`, `cm` and `pyplot` from `matplotlib`, `numpy`, `sys` and `os`. The module `matplotlib` (<http://matplotlib.org/>) is used for the visualization of the design. The module `dolfin` is a problem-solving environment required to use FEniCS. The purpose of the line

```
10 pyplot.switch_backend('Agg')
```

is to use the `Agg` backend instead of the default `WebAgg` backend. With the `Agg` backend, the figures do not appear on the screen, but are saved to a file; see lines 121-128.

**6.1. Initialization of case-dependent parameters.** The file `init.py` provides initial data which depends on the chosen case. The outputs of this file are the variables which are case-dependent, i.e. `LagVol`, `Nx`, `Ny`, `lx`, `ly`, `LoadCase`, `NameCase`, `ds`, `bcd`, `mesh`, `phi_mat`. The function space `V1vec` is not case-dependent but is required to define the boundary conditions `bcd`.

The Lagrange multiplier  $\Lambda$  for the volume constraint is called here `LagVol`. The variable `LoadCase` is the position of the pointwise load, for example for the cantilever it is `LoadCase = [Point(lx, 0.5)]`, which means that the load is applied at the point  $(l_x, 0.5)$ . For the asymmetric cantilever we have `LoadCase = [Point(lx, 0.0)]`.

The fixed domain  $\mathcal{D}$  is a rectangle  $\mathcal{D} = [0, l_x] \times [0, l_y]$ . In the code this corresponds to the variables `lx`, `ly`. The mesh is built using the line

```
mesh = RectangleMesh(Point(0.0,0.0),Point(lx,ly),Nx,Ny,'crossed')
```

The class `RectangleMesh` creates a mesh in a 2D rectangle spanned by two points (opposing corners) of the rectangle. The arguments `Nx`, `Ny` specify the number of divisions in the  $x$ - and  $y$ -directions, and the optional argument `crossed` means that the diagonals are crossed. One should choose `lx`, `ly`, `Nx`, `Ny` with the constraint  $lx \cdot Nx^{-1} = ly \cdot Ny^{-1}$  in order to keep the elements isosceles. The choice of the argument `crossed` is necessary to have a symmetric displacement  $u$  and in turn to keep a symmetric design throughout the iterations if the problem is symmetric, for instance in the case of the cantilever. Note that to preserve the symmetry of solutions at all time, one must choose an odd number of divisions `Nx` or `Ny`, depending on the orientation of the symmetry. For instance, in the case of the cantilever, one can choose `Ny=75` since the symmetry axis is the line  $y = 1/2$ , and `Nx=150`.

Since we chose a mesh with crossed diagonals, each square has an additional vertex at its center, where the diagonals meet. Therefore the total number of vertices is

```
47 dofsV1_max = (Nx+1)*(Ny+1) + Nx*Ny
```

We also define `dofsV1vec_max = 2*dofsV1_max` which represents the degrees of freedom for the vector function space `V1vec`; see line 47.

The case-dependent boundary  $\Gamma_d$  is defined using the class `DirBd`, and instantiated by `dirBd = DirBd()`. We tag `dirBd` with the number 1, the other boundaries with 0, and introduce the boundary measure `ds`. The Dirichlet boundary condition on  $\Gamma_d$  is defined using

```
DirichletBC(V1vec, (0.0,0.0), boundaries, 1)
```

The variable `bcd` is a vector of boundary conditions, in case there are several types of Dirichlet boundary conditions, as in the case of the half-wheel. In the case of the cantilever, `bcd` has only one element.

**6.2. Other initialization parameters.** The ersatz material coefficient  $\epsilon$  of (27) is called `eps_er`. For the elasticity parameters  $E, \nu, \mu, \lambda$  the variables are given lines 16-17. In line 18-21, new directories are created to save the results. For the line search, `ls_max = 3` is the maximum number of line searches for one iteration of the main loop, `ls` is an iteration counter for the line search. The step size used in the gradient method is `beta`, which is initialized as `beta0_init`. We choose `beta0_init = 0.5`. We also choose `gamma = 0.8` and `gamma2 = 0.8`, which are used to modify the step size in the line search; see Section 6.8.

The counter `Iter` on line 27 keeps track of the iterations of the main loop. We also fix a maximum number of iterations `IterMax = int(1.5*Nx)`, which depends on `Nx` since the number of iterations increases with the mesh size.

**6.3. Finite elements.** In line 30 and in the file `init.py`, we define the following finite element spaces associated with `mesh`:

```
V1 = FunctionSpace(mesh, 'CG', 1)
V1vec = VectorFunctionSpace(mesh, 'CG', 1)
```

Here, `CG` is short for “continuous Galerkin”, and the last argument is the degree of the element, meaning we have chosen the standard linear Lagrange element. Note that the type of elements and degree can be easily modified using this command, and FEniCS offers a variety of them. However, the level set part of our code has been written for this particular type of elements, so changing it would require to modify other parts of the code, such as the function `_comp_lsf`, so one should be aware that it would not be a straightforward modification.

**6.4. Level set function.** In lines 33-40, we define matrices which are used to compute the finite differences of the level set function  $\phi$ . Indeed, it is important to understand that we use two separate grids in this code. On one

hand, `mesh` is used to solve the solution  $U$  of the elasticity system and the vector field  $\theta$ , represented by `th` in our code, whereas on the other hand the level set function  $\phi$  is defined on a Cartesian grid. We have seen that the Hamilton-Jacobi equation (40) determining the evolution of  $\phi$  requires the calculation of the finite differences  $D_x^\pm \phi_{ij}$  and  $D_y^\pm \phi_{ij}$ . In our code, the matrices `Txm`, `Txp`, `Typ`, `Tym` in lines 33-40 are precisely the matrices which allow to compute these finite differences. For instance `Txm` is associated with  $D_x^- \phi$  (here the `m` in `Txm` stands for 'minus' and the `p` in `Txp` for 'plus'). In line 164, one can see how `Txm` is used to compute `Dxm` which corresponds to  $D_x^- \phi$ :

```
164 Dxm = ( Nx*(np.dot(psi,Txm)) )/lx
```

The `numpy` command `np.dot` is simply a matrix product in this case. Note that there is an issue for computing certain finite differences on the boundary of  $\mathcal{D}$ , since we would need values outside of  $\mathcal{D}$ . To solve this issue, we use a linear extrapolation of the value of  $\phi$  outside of  $\mathcal{D}$ . For instance for `Txm`, this extrapolation corresponds to `Txm[0:2,0] = [-1,1]` in line 34, and similarly for the other matrices, see lines 36, 38 and 40.

Another important observation is that there are two incarnations of the level set function  $\phi$  in our code because of the two different grids: `phi` is a function defined on `mesh`, while `phi_mat` is the function defined on the Cartesian grid. Obviously, we need mechanisms to alternate between `phi` and `phi_mat`. In fact we only need to get `phi` from `phi_mat`, indeed `phi_mat` is updated every iteration by the function `_hj`, and we need `phi` to define the new set  $\Omega$  in lines 52-54. Observe that the set of vertices of the Cartesian grid is included in the set of vertices of `mesh`, indeed the vertices of `mesh` are precisely the vertices of the Cartesian grid, plus the vertices in the center of the squares where the diagonals meet, due to the choice of the argument `crossed` in `mesh`. Therefore we need to interpolate the values of `phi_mat` at the center of the squares. This is simply done in the function `_comp_lsf` (lines 196-208) by taking the mean value of the four vertices of each square to define the value at the center; see lines 203-206. In lines 201-202, we set the values of `phi` to be equal to the values of `phi_mat` at the vertices which are common between `mesh` and the Cartesian grid. Thus the output of `_comp_lsf` is the function `phi` defined on `mesh`. Note that if we had chosen squares with just one diagonal (choosing `left` or `right` instead of `crossed` in `RectangleMesh` in the file `init.py`) instead of two, there would be an exact correspondence between `phi` and `phi_mat`, so that switching between the two would be trivial. However, we chose `crossed` to preserve the symmetry of the problem, as explained above.

In lines 42-47, `dofsV1` and `dofsV1vec` are the coordinates of the vertices associated with the degrees of freedom. Using `dofsV1` and `dofsV1vec` we define `plx`, `ply` and `plvec_x`, `plvec_y`, respectively, which have integer values and are used by `_comp_lsf` to find the correspondence between the entries of the matrix `phi_mat` and the entries of `phi`. In `_comp_lsf`, line 200, we check if the vertex associated with `plx`, `ply` corresponds to a vertex on the Cartesian grid or to the center of a square, and we build the vector `phi` accordingly.

**6.5. Initialization of the level set function.** In lines 49-50, we initialize `phi` as a function in the space `V1`, and using `_comp_lsf` we determine its entries using `phi_mat`. The matrix `phi_mat` is initialized in the file `init.py`, since it is case-dependent. For instance, for the cantilever we chose

$$(50) \quad \begin{aligned} \phi(x, y) = & -\cos(8\pi x/l_x) \cos(4\pi y) - 0.4 + \max(200(0.01 - x^2 - (y - l_y/2)^2), 0) \\ & + \max(100(x + y - l_x - l_y + 0.1), 0) + \max(100(x - y - l_x + 0.1), 0), \end{aligned}$$

which is the initialization yielding the result in Figure 1. Clearly, the coefficients inside the cosine determine the initial number of “holes” inside the domain (i.e. the number of connected components of  $\mathcal{D} \setminus \Omega$ ). Here (50) corresponds to ten initial holes inside the domains (plus some half-holes on the boundary of  $\mathcal{D}$ ), as can be seen in Figure (7).

The reason for the additional three `max` terms in (50) is specific of our approach. The main idea is that one should not put material in certain parts of the domain, in particular certain corners of  $\mathcal{D}$ . The explanation is the following. Since the perturbation field  $\theta$  is defined by a problem on all of  $\mathcal{D}$ , the question of boundary conditions on  $\partial\mathcal{D}$  for the PDE determining  $\theta$  is crucial. Indeed by definition, the set  $\Omega$  should satisfy the constraint  $\Omega \subset \mathcal{D}$ . This logically implies the boundary conditions  $\theta = 0$  on  $\Gamma_d$  and  $\theta \cdot n \leq 0$  on  $\partial\mathcal{D} \setminus \Gamma_d$ , where  $n$  is the outward normal vector to  $\mathcal{D}$ . However, from a numerical point of view, the latter condition is impractical, since one would have to solve a variational inequality at each iteration. We found that the stronger condition  $\theta \cdot n = 0$  on  $\partial\mathcal{D}$  was a good compromise, as it allows for tangential movements of the shape along  $\partial\mathcal{D}$ , unfortunately this condition leads to  $\theta = 0$  in the corners of  $\mathcal{D}$ . Therefore the shape in a small neighbourhood of the corners will not change, and if we start with an inappropriate initialization, we will end with a small set of unwanted material in certain corners. Therefore the rôle of the `max`-terms in (50) is to create a small cut with the correct material in certain corners. Depending on the problem, it is easy to see what should be the correct corner material distribution for the final design.

Another problem may appear at boundary points which are on the symmetry axis for symmetric problems. Indeed, due to the smoothness of  $\theta$  and the symmetry of the problem, we will get  $\theta_x = 0$  or  $\theta_y = 0$  at these points and the shape will not change there. For instance in the symmetric cantilever case, this problem happens at the point  $[0, l_y/2]$ . There is no issues at  $[l_x, l_y/2]$ , since this is the point where the load is applied, so it must be fixed anyway. This explain the term  $\max(200(0.01 - x^2 - (y - l_y/2)^2), 0)$  in (50).

In lines 52-54 we define the class `Omega` of the set of points where `phi` is negative. In line 56 we define the integration measure `dx` on  $\mathcal{D}$ . In line 57 the normal vector `n` to  $\mathcal{D}$  is introduced to define the boundary conditions for `Av` in line 61.

**6.6. Assembling the matrix for the descent direction.** In lines 59-62, we define the matrix `av` which corresponds to the bilinear form (37). FEniCS uses the Unified Form Language (UFL) for representing weak formulations of partial differential equations, which results in an intuitive notation, close to the mathematical one. This can be seen in lines 60-61, where the bilinear form of (37) is given by

```
60 Av = (1.0*inner(grad(theta),grad(xi)) + 0.1*inner(theta,xi)) * dx\
61      + 1.0e4*(inner(dot(theta,n),dot(xi,n)) * (ds(0)+ds(1)+ds(2)))
```

Here `theta` and `xi` are functions in `V1vec`, `xi` is the test function in (36), while `theta` corresponds to  $\theta$  in (36). In our code, we use the notation `th` for  $\theta$  when  $\theta$  is the descent direction, and `th` belongs to the space `V1vec`. The choice of boundary conditions for `Av`, which are modeled by the part

```
61 1.0e4*(inner(dot(theta,n),dot(xi,n)) * (ds(0)+ds(1)+ds(2)))
```

is explained in Section 6.5. For cases where `dirBd2` is not defined, such as the cantilever case, the term `+ds(2)` has no effect.

Note that we assemble the matrix for the PDE of `th` in line 62, i.e. before the start of the main loop. Indeed, the bilinear form  $\mathcal{B}$  in (37) is independent of  $\Omega$ . Thus, since we use a LU factorization to compute  $\theta$ , we can reuse the factorization every iteration to solve the PDE for `th`, see lines 157-159. This allows to spare a substantial amount of calculations, but for grids larger than the ones considered in this paper, it would be appropriate to use more efficient approaches such as Krylov methods to solve the PDE. This can be done easily with FEniCS using one of the various available solvers.

**6.7. Update domain and cost functional.** The main loop starts line 64. In line 66 we instantiate by `omega = Omega()`. This either initializes `omega` or updates `omega` if `phi` has been updated inside the loop. In line 68, `omega` is tagged with the number 1, so that we can integrate on `omega` using `dx(1)`. The complementary of `omega` is tagged with the number 0 in line 67. Note that the measure `dx` (line 56) allows to integrate on all of  $\mathcal{D}$ . We define the integration measure for the subdomains  $\Omega$  and  $\mathcal{D} \setminus \Omega$  using

```
69 dx = Measure('dx')(subdomain_data = domains)
```

One assembles using `dx(1)` to integrate on  $\Omega$ , and using `dx(0)` to integrate on  $\mathcal{D} \setminus \Omega$ ; see for instance lines 77-79. For details on how to integrate on specific subdomains and boundaries, we refer to the FEniCS documentation.

Then we can compute `U`, the solution of the elasticity system in lines 70-72. Note that `U` is a vector since we consider the general case of several loads. Thus the length of the vector is the length of `LoadCase`; see line 70. In lines 74-81 we compute the compliance, the volume of `omega` and the cost functional  $\mathcal{J}$ . Again, observe that the command for the calculation of the compliance is close to the mathematical notation, i.e. it resembles the following mathematical formula of the compliance:

$$\mathcal{J}(\Omega) = \int_{\mathcal{D}} A_{\Omega} e(u) \cdot e(u) = \int_{\Omega} 2\mu e(u) \cdot e(u) + \lambda \operatorname{tr}(e(u))^2 + \epsilon \int_{\mathcal{D} \setminus \Omega} 2\mu e(u) \cdot e(u) + \lambda \operatorname{tr}(e(u))^2.$$

Note that the compliance is a sum in the case of several loads, hence the `for` loop in line 75.

**6.8. Line search and stopping criterion.** The line search starts at line 83. If the criterion

$$\mathcal{J}[\text{Iter}] > \mathcal{J}[\text{Iter}-1]$$

is satisfied, then we reject the current step. In this case we reduce the step size `beta` by multiplying it by  $\gamma$  in line 85. Also, we go back to the previous values of `phi_mat` and `phi` which were stored in `phi_mat_old` and `phi_old`, see line 86. Then we need to recalculate `phi_mat` and `phi` in lines 87-88 using the new step size `beta`.

If the step is not rejected, then we go to the next iteration starting from line 96. If the step was accepted in the first iteration of the line search, in order to speed up the algorithm we increase the reference step size `beta0` by setting

```
beta0 = min(beta0 / gamma2, 1)
```

to take larger steps, since `gamma2` is smaller than one. Here the reason why `beta0` should not exceed the value 1 is the CFL condition for the time step `dt` in line 171. We chose `gamma2 = 0.8` in our examples; see line 23.

If the maximum number of line searches `ls_max` is reached, we decrease in line 96 the reference step size `beta0` by setting

```
beta0 = max(beta0 * gamma2, 0.1 * beta0_init)}
```

We impose the lower limit `0.1*beta0_init` on `beta0` so that the step size does not become too small. Note that `beta` is reseted to `beta0` in line 99.

**6.9. Descent direction.** In line 101, we compute the descent direction `th`. The function `_shape_der` in lines 146-160 solves the PDE for  $\theta$ , i.e. it implements (36)-(37) using the volume expression of the shape derivative (32)-(33). Also taking into account the volume constraint, the variational formulation used in our code for the case of one load is: find  $\theta \in H_d^k(\mathcal{D})^m$  such that

$$(51) \quad \int_{\mathcal{D}} \alpha_1 D\theta \cdot D\xi + \alpha_2 \theta \cdot \xi = - \int_{\mathcal{D}} (2Du^T A_{\Omega} e(u) - A_{\Omega} e(u) \cdot e(u) I_d) \cdot D\xi - \Lambda \int_{\Omega} \operatorname{div} \xi, \quad \text{for all } \xi \in H^1(\mathcal{D})^m.$$

with  $\alpha_1 = 1$  and  $\alpha_2 = 0.1$ . When several loads are applied, as in the case of `cantilever_twoforces`, the right-hand side in (51) should be replaced by a sum over the loads `u` in `u_vec`.

In lines 151-155, observe that the implementation of the involved expression of the distributed shape derivative is close to the mathematical formulation (51), but we need to integrate separately on  $\Omega$  and  $\mathcal{D} \setminus \Omega$  using `dx(1)` and `dx(0)`, respectively. We use a `LUSolver` to solve (51). The parameter `reuse_factorization` in line 158 allows to reuse the LU factorization of the matrix `av`, assembled in line 62, since `av` does not change.

Line 101 yields the descent direction `th` in the space `V1vec`. To update `phi` we need to have `th` on the Cartesian grid. As we explained already, we just need to extract the appropriate values of `th` since the Cartesian grid is included in `mesh`. This is what is done in lines 102-111, and the corresponding function on the Cartesian grid, which is a matrix, is called `th_mat`.

**6.10. Update level set function.** Once we have calculated `th` and defined the corresponding `th_mat` on the Cartesian grid, we proceed to update the level set function `phi_mat_new` using the subfunction `_hj`. Note that the suffix `_mat` in our code denotes quantities defined on the Cartesian grid. The subfunction `_hj` in lines 162-173 follows exactly the discretization procedure described in Section 5.2. In lines 164-167, the quantities `Dxm`, `Dxp`, `Dyp`, `Dym` correspond to  $p^-$ ,  $p^+$ ,  $q^+$ ,  $q^-$ , respectively. In line 163, we take 10 steps of the Hamilton-Jacobi update, which is a standard, although heuristic way, to accelerate the convergence. In line 171, the time step is chosen, according to the CFL condition, as

```
171 dt = beta*lx / (Nx*maxv)
```

since we have the step size `beta` smaller than 1 at all time in view of line 97. In line 115, the function `phi_new` is extrapolated from `phi_mat_new` using `_comp_lsf`. In line 116, we save the current versions of `phi` and `phi_mat` in the variables `phi_old`, `phi_mat_old`, for use in case the step gets rejected during the line search.

**6.11. Reinitialization of the level set function.** Every 5 iterations, we reinitialize the level set function at line 114. This is achieved by the subfunction `_reinit` in lines 175-194. The reinitialization follows the procedure described in Section 5.3. In lines 184-187, `Dxm`, `Dxp`, `Dyp`, `Dym` correspond to  $p^-$ ,  $p^+$ ,  $q^+$ ,  $q^-$ , respectively. In lines 188 to 191, `Gp` and `Gm` correspond to  $G^+$  and  $G^-$  from (48)-(49), respectively. Line 192 corresponds to (47) and line 193 to the update (46).

The function `signum`, computed in line 178, is the approximation of the sign function of  $\phi$  corresponding to  $S(\phi)$ , defined in (45). To compute `signum`, we use `lx/Nx` for  $\epsilon$ , and  $|\nabla \phi|$  is computed using symmetric finite differences  $\phi$ , which are given by `Dxs` and `Dys` in lines 176-177.

**6.12. Stopping criterion and saving figures.** Finally in lines 119-120, we check if the stopping criterion

```
max(abs(J[Iter-5:Iter] - J[Iter-1])) < (2.0/Nx**2) * J[Iter-1]
```

is satisfied. Here, `Iter-1` is the current iteration. This means that the algorithm stops when the maximum difference of the value of the cost functional at the current iteration with the values of the four previous iterations is below a certain threshold. In order to take smaller steps when the grid gets finer, we have determined heuristically the threshold  $(2.0/Nx**2) * J[Iter-1]$  which depends on the grid size `Nx`.



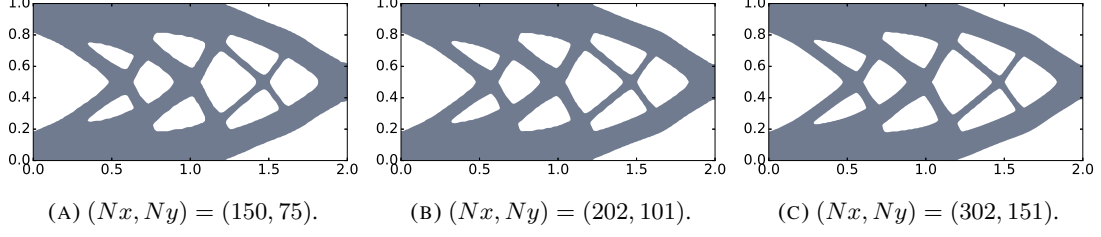


FIGURE 1. Optimal design for the symmetric cantilever, with  $\Lambda = 40$ , and initialization (50).

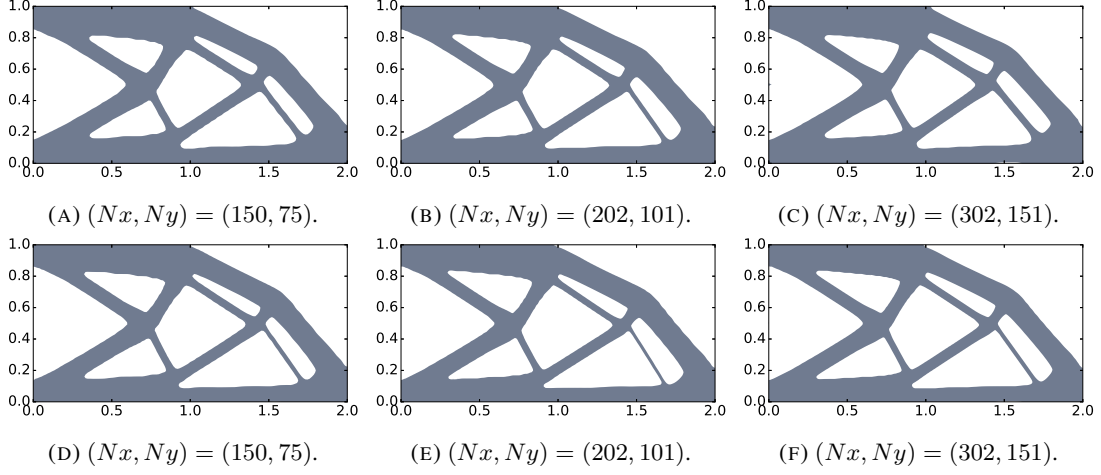


FIGURE 2. Asymmetric cantilever, first row:  $\Lambda = 60$ , second row:  $\Lambda = 70$ .

Lines 122-128 are devoted to plotting the design, drawing the filled contour of the zero level set of `phi_mat` using the `pyplot` function `contourf`, see the `matplotlib` documentation for details.

## 7. NUMERICAL RESULTS AND CASE-DEPENDENT PARAMETERS

We recall that the parameters which are specific to each case can be found in the file `init.py`. In this section we discuss the case-dependent parameters which we have used such as boundary conditions, load position, and Lagrangian  $\Lambda$ .

**7.1. Symmetric cantilever.** For the symmetric cantilever the load is placed at the point  $(l_x, l_y/2)$ , see the parameter `LoadCase`. The initialization for the symmetric cantilever is given by (50). See Figure 1 for the results of the symmetric cantilever for several grid sizes and  $\Lambda = 40$ . See also Figure 7 for a comparison of two different initializations. We observe that the optimal set is independent of the mesh size but depends on the initialization.

To obtain a short symmetric cantilever, one can set `lx = ly` and `Nx = Ny`. Still, one should choose an odd number for `Nx` in order to preserve the symmetry of the problem.

**7.2. Asymmetric cantilever.** For the asymmetric cantilever, we take `LoadCase = [Point(lx, 0.0)]`, to have a load in the lower right corner. The initialization is also changed, so as to start with the material phase where the load is applied, more precisely, we choose

$$\phi(x, y) = -\cos(6\pi x/l_x) \cos(4\pi y) - 0.4 + \max(100(x + y - l_x - l_y + 0.1), 0).$$

See Figure 2 for the results of the asymmetric cantilever for several grid sizes, for  $\Lambda = 60$  and  $\Lambda = 70$ .

**7.3. Half-wheel.** For the half-wheel we have `lx, ly = [2.0, 1.0]`. We need pointwise Dirichlet conditions in the corner  $(0.0, 0.0)$  and rolling conditions in  $(l_x, 0.0)$ . This is achieved by using the following boundaries:

```
class DirBd(SubDomain):
    def inside(self, x, on_boundary):
        return abs(x[0]) < tol and abs(x[1]) < tol
class DirBd2(SubDomain):
    def inside(self, x, on_boundary):
```



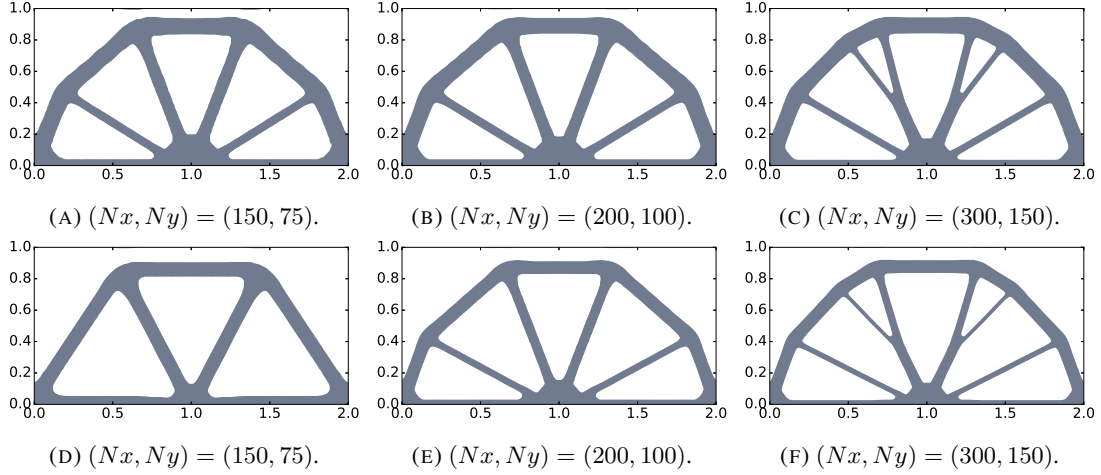


FIGURE 3. Optimal design for the half-wheel,  $\Lambda = 30$  (first row),  $\Lambda = 50$  (second row).

```
return abs(x[0]-lx) < tol and abs(x[1]) < tol
dirBd, dirBd2 = [DirBd(), DirBd2()]
```

where  $\text{tol} = 1\text{E-}14$ . Then the two boundary parts are tagged with different numbers

```
dirBd.mark(boundaries, 1)
dirBd2.mark(boundaries, 2),
```

and we define the vector of boundary conditions as

```
bcd = [DirichletBC(V1vec, (0.0,0.0), dirBd, method='pointwise'), \
        DirichletBC(V1vec.sub(1), 0.0, dirBd2, method='pointwise')]
```

The method `pointwise` is used since `dirBd2` is a single point. Note here that the rolling boundary condition is achieved by setting the component `V1vec.sub(1)` to 0, indeed `V1vec.sub(1)` represents the  $y$ -component of a vector function taken in the space `V1vec`. In lines 60-61 of `compliance.py`, Dirichlet conditions for  $\theta$  are applied on `dirBd` and `dirBd2` as these corners should be fixed.

The initialization should also change to fit the half-wheel case. We chose

```
phi_mat = -np.cos((3.0*pi*(XX-1.0))) * np.cos(7*pi*YY) - 0.3 +
            np.minimum(5.0/ly * (YY-1.0) + 4.0, 0) \
            + np.maximum(100.0*(XX+YY-lx-ly+0.1), .0) + np.maximum(100.0*(-XX+YY-ly+0.1), .0)
```

The position of the load is given by `LoadCase = [Point(lx/2, 0.0)]`. In Figure 3 we compare results obtained with  $\Lambda = 30$  and  $\Lambda = 50$ .

**7.4. Bridge.** The case of the bridge is similar to the case of the half-wheel. The main difference is the pointwise Dirichlet condition in the lower right corner, which corresponds to

```
bcd = [DirichletBC(V1vec, (0.0,0.0), dirBd, method='pointwise'), \
        DirichletBC(V1vec, (0.0,0.0), dirBd2, method='pointwise')]
```

Also for the initialization we take

```
phi_mat = -np.cos((4.0*pi*(XX-1.0))) * np.cos(4*pi*YY) - 0.2 \
            + np.maximum(100.0*(YY-ly+0.05), .0)
```

See Figure 4 for numerical results for the bridge, with  $\Lambda = 20$  and  $\Lambda = 30$ .

**7.5. MBB-beam.** We define the MBB beam as in the original paper [52]. First of all we take  $lx=3.0$  and  $ly=1.0$ , and  $N_x, N_y$  must be chosen accordingly, so as to keep a regular grid. For instance, we can choose  $N_x=150, N_y=50$ . We take `LoadCase = [Point(0.0, 1.0)]`. On the left side of the domain  $\mathcal{D}$  we have rolling

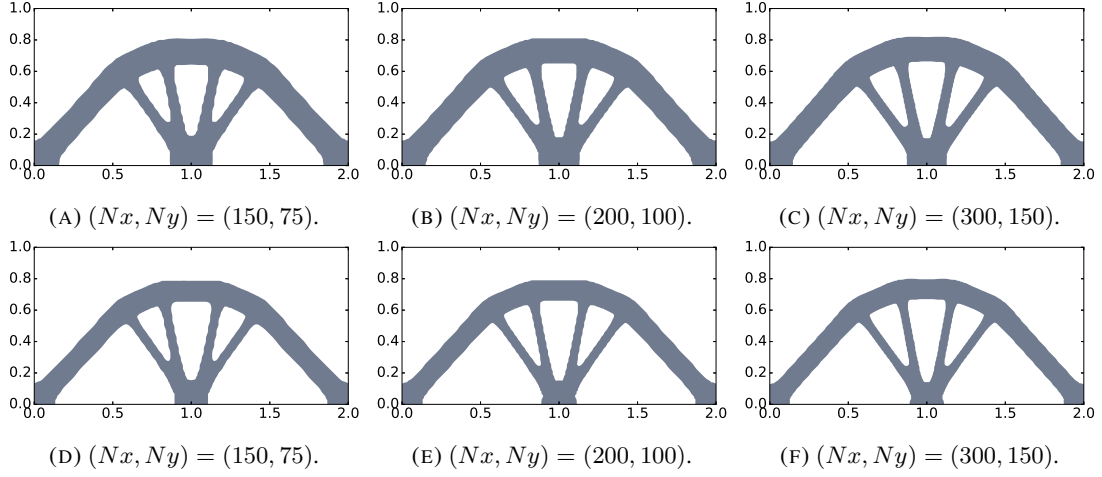


FIGURE 4. Optimal design for the bridge, with  $\Lambda = 20$  (first row) and  $\Lambda = 30$  (second row).

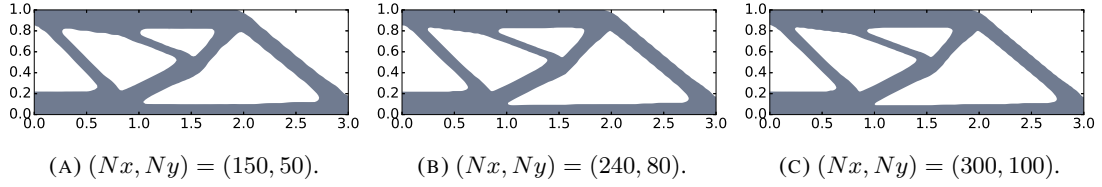


FIGURE 5. Optimal design for the MBB-Beam,  $\Lambda = 130$ .

boundary condition, which corresponds to  $u \cdot n = 0$ , we also have pointwise rolling boundary conditions on the lower right corner of  $\mathcal{D}$ . In `init.py` this corresponds to the following definitions of the boundaries:

```
class DirBd(SubDomain):
    def inside(self, x, on_boundary):
        return near(x[0], .0)
class DirBd2(SubDomain):
    def inside(self, x, on_boundary):
        return abs(x[0]-lx) < tol and abs(x[1]) < tol
dirBd, dirBd2 = [DirBd(), DirBd2()]
```

Then the two boundary parts are tagged with different numbers

```
dirBd.mark(boundaries, 1)
dirBd2.mark(boundaries, 2)
```

Then we define the boundary conditions on the two boundaries `dirBd` and `dirBd2`:

```
bcd = [DirichletBC(V1vec.sub(0), 0.0, boundaries, 1), \
        DirichletBC(V1vec.sub(1), 0.0, dirBd2, method='pointwise')]
```

Also, the term `+ds(2)` in lines 60-61 of `compliance.py` is active since `dirBd2` is not empty, as for the half-wheel case. We also choose an appropriate initialization

```
phi_mat = -np.cos(4.0/lx*pi*XX) * np.cos(4.0*pi*YY) - 0.4 \
    + np.maximum(100.0*(XX+YY-lx-ly+0.1), .0) + np.minimum(5.0/ly * (YY-1.0) + 4.0, 0)
```

We illustrate the MBB-Beam case with  $\Lambda = 130$  in Figure 6.

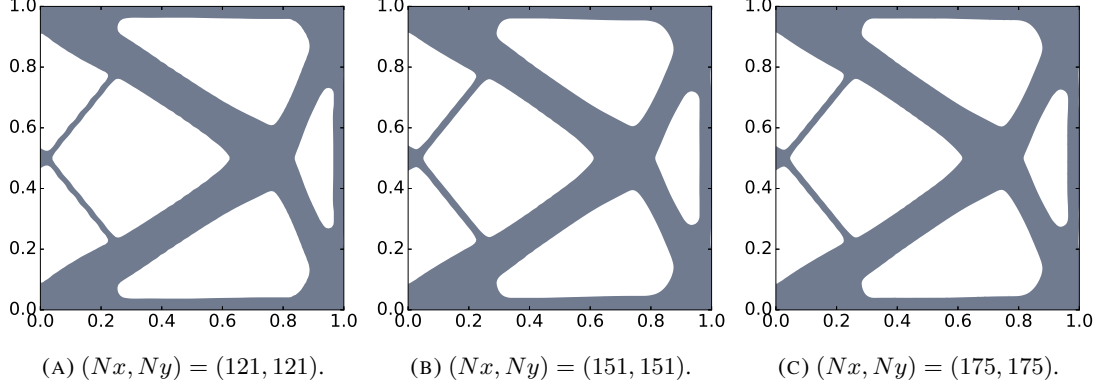


FIGURE 6. Optimal design for the cantilever with two loads with  $\Lambda = 60$ .

**7.6. Multiple load case.** In the case of multiple loads, we have a set of forces  $\{g_i\}_{i \in I}$  and the compliance is the sum of the compliances associated to each force  $g_i$ :

$$J(\Omega) := \sum_{i \in I} \int_{\Gamma_n} g_i \cdot u_i,$$

where  $u_i$  is the solution of the linearized elasticity corresponding to  $g_i$ . We have for this case that

```
LoadCase = [Point(lx, 0.0), Point(lx, 1.0)]
```

is a vector. In line 70 of `compliance.py`,  $U$  is thus a vector of two components corresponding to the two different loads. It is clear that the shape derivative is also a sum in this case, for instance using the shape derivative formula (24) we obtain

$$(52) \quad dJ^{\text{vol}}(\Omega; \theta) = \sum_{i \in I} \int_{\Omega} S_1^i \cdot D\theta,$$

with

$$S_1^i := 2Du_i^T Ae(u_i) - Ae(u_i) \cdot e(u_i)I_d.$$

Therefore, when solving (36) to find a descent direction, we just need to sum the right-hand sides using (52). This explains the `for` loop in the function `_shape_der`.

We illustrate the multiple load case with a cantilever problem with two loads applied at the bottom-right corner and the top-right corner, both with equal intensities to get a symmetric design. Here the Lagrangian is taken as  $\Lambda = 60$ . The results are shown in Figure 6. We use the initialization

```
phi_mat = -np.cos(4.0*pi*(XX-0.5)) * np.cos(4.0*pi*(YY-0.5)) - 0.6 \
- np.maximum(50.0*(YY-ly+0.1), .0) - np.maximum(50.0*(-YY+0.1), .0)
```

## 8. INITIALIZATION AND COMPUTATION TIME

**8.1. Influence of initialization.** It is known that the final result may depend on the initial guess for the minimization of the compliance. We observe this phenomenon in our algorithm, this is illustrated in Figure 7, where two different initializations provide two different optimal designs. We compare initialization (50) with

$$(53) \quad \begin{aligned} \phi(x, y) = & -\cos(6\pi x/l_x) \cos(4\pi y) - 0.6 + \max(200(0.01 - x^2 - (y - l_y/2)^2), 0) \\ & + \max(100(x + y - l_x - l_y + 0.1), 0) + \max(100(x - y - l_x + 0.1), 0). \end{aligned}$$

The choice  $\phi(x, y) = -\cos(6\pi x/l_x) \cos(4\pi y) - 0.6$  corresponds to a standard choice of seven holes inside the domain for the  $2 \times 1$  cantilever; see [40]. It can be seen in Figure 7 that the initialization with the higher number of holes provides a more complicated optimal design where the set  $\mathcal{D} \setminus \Omega$  has more connected components.

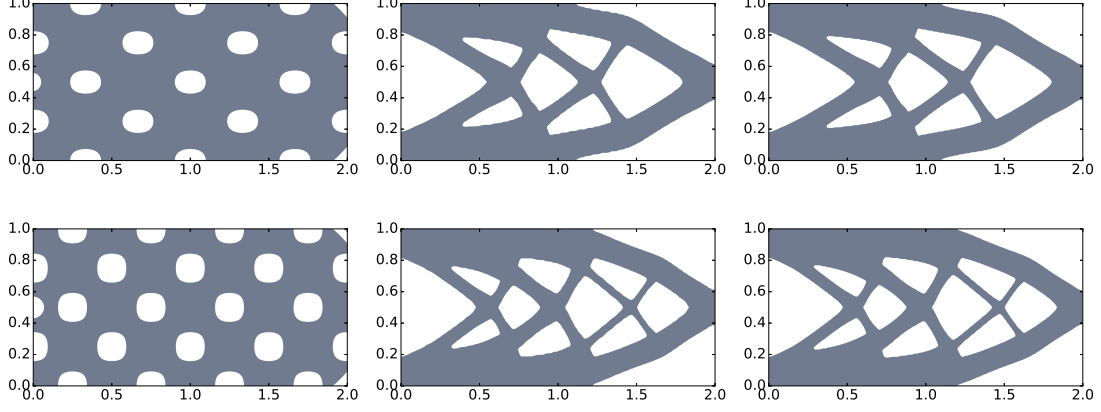


FIGURE 7. Optimal design for the symmetric cantilever, with  $\Lambda = 40$  and two different initial guesses. First column: initial guess, second column: optimal design for  $(N_x, N_y) = (202, 101)$ , third column: optimal design for  $(N_x, N_y) = (302, 151)$ . The first line uses initialization (53), the second line uses initialization (50).

TABLE 1. Computation time for the asymmetric cantilever benchmark for  $\Lambda = 60$ .

Mesh size	$102 \times 51$	$150 \times 75$	$202 \times 101$	$302 \times 151$
Number of elements	10,558	22,726	41,108	91,658
IterMax	153	225	303	453
Total number of iterations	72	130	303	377
Average time for one iteration (seconds)	1.99	4.35	8.35	19.29
Total time until convergence (h:m:s)	0:04:18	0:13:34	1:07:33	2:19:41

**8.2. Computation time.** The numerical tests were ran on a PC with four processors Intel Core2 Q9400, 2.66 GHz, 3.8 GB memory, with LinuxMint 17 and FEniCS 2016.2. In Tables 1 and 2 we show the computation time for the symmetric and asymmetric cantilevers. The average time for one iteration is computed by averaging over all iterations. However, it is not counting the time spent during the initialization, and the time spent when the line search is performed, i.e. the time is recorded only for steps which are accepted.

Since we use a mesh with crossed elements, the number of elements is

$$\text{dofsV1}_{\max} = (N_x + 1) * (N_y + 1) + N_x * N_y$$

We solve two partial differential equations during each iteration (again, without counting the line search, and assuming we have only one load), one to compute  $\mathbf{u}$ , and one to compute  $\mathbf{t}_h$ . Since these are vectors, the number of degrees of freedom for solving each of these PDEs is therefore

$$2 * \text{dofsV1}_{\max} = 2 * ((N_x + 1) * (N_y + 1) + N_x * N_y)$$

For instance for the case  $(N_x, N_y) = (302, 151)$ , as in Table 1, we get 91,658 elements and 183,316 degrees of freedoms. When comparing with the computational time for an algorithm such as the one described in [8], one should use the number of elements as the basis for comparison. For example, a  $300 \times 100$  mesh in [8] gives 30,000 elements, which corresponds approximatively to a grid of  $170 \times 85$  which gives 29,156 elements for our code.

Comparing with the results in [8], the computation time is comparable, although slightly slower, for the same number of elements. Comparing with the educational code from [16], which is also based on the level set method, our code is significantly faster. Indeed, it was observed in [28] that the code of [16] takes a long time to converge if the mesh discretization is greater than 5,000 elements. In [28] the authors have improved its efficiency by using a sparse matrix assembly, but they did not report on computation time.

TABLE 2. Computation time for the symmetric cantilever benchmark for  $\Lambda = 40$ .

Mesh size	$102 \times 51$	$150 \times 75$	$202 \times 101$	$302 \times 151$
Number of elements	10,558	22,726	41,108	91,658
IterMax	153	225	303	453
Total number of iterations	60	84	82	247
Average time for one iteration (seconds)	2.04	4.45	8.64	19.56
Total time until convergence (h:m:s)	0:04:48	0:13:26	0:18:00	2:19:18

**Acknowledgment.** The author acknowledges the support of the Brazilian National Council for Scientific and Technological Development (Conselho Nacional de Desenvolvimento Científico e Tecnológico - CNPq), through the program “Bolsa de Produtividade em Pesquisa - PQ 2015”, process: 302493/2015-8.

## 9. APPENDIX: FENICS CODE compliance.py

```

1  # -----
2  # FEniCS code for level set-based structural optimization.
3  # Written by Antoine Laurain, 2017
4  # -----
5  from dolfin import *
6  from init import *
7  from matplotlib import cm, pyplot
8  import numpy as np
9  import sys, os
10 pyplot.switch_backend('Agg')
11 set_log_level(ERROR)
12 # -----
13 def _main():
14     LagVol, Nx, Ny, lx, ly, LoadCase, NameCase, ds, bcd, mesh, phi_mat, V1vec\
15     = initialize(sys.argv[1])
16     eps_er, E, nu = [0.001, 1.0, 0.3] # Elasticity parameters
17     mu, lmbda = Constant(E/(2*(1 + nu))), Constant(E*nu/((1 + nu)*(1 - 2*nu)))
18     # Create folder for saving files
19     results_dir = os.path.join(os.path.dirname(__file__), \
20     NameCase + '/LagVol=' + str(np.int_(LagVol)) + '_Nx=' + str(Nx) )
21     if not os.path.isdir(results_dir): os.makedirs(results_dir)
22     # Line search parameters
23     beta0_init, ls, ls_max, gamma, gamma2 = [0.5, 0.3, 0.8, 0.8]
24     beta0 = beta0_init
25     beta = beta0
26     # Stopping criterion parameters
27     IterMax, Iter, stop_criter = [int(1.5*Nx), 0, False]
28     # Cost functional and function space
29     J = np.zeros( IterMax )
30     V1 = FunctionSpace(mesh, 'CG', 1)
31     VolUnit = project(Expression("1.0", degree=2), V1) # To compute volume
32     # Matrices to compute finite differences of phi
33     Txm = np.eye(Nx+1, Nx+1, 0) - np.eye(Nx+1, Nx+1, 1)
34     Txm[0:2, 0] = [-1, 1]
35     Txp = -np.eye(Nx+1, Nx+1, 0) + np.eye(Nx+1, Nx+1, -1)
36     Txp[Nx-1:Nx+1, Nx] = [-1, 1]
37     Typ = -np.eye(Ny+1, Ny+1, 0) + np.eye(Ny+1, Ny+1, 1)
38     Typ[Ny-1:Ny+1, Ny] = [-1, 1]
39     Tym = np.eye(Ny+1, Ny+1, 0) - np.eye(Ny+1, Ny+1, -1)

```

```

40 Tym[0,0:2] = [-1,1]
41 # Get vertices coordinates
42 gdim = mesh.geometry().dim()
43 dofsV1 = V1.tabulate_dof_coordinates().reshape((-1, gdim))
44 dofsV1vec = V1vec.tabulate_dof_coordinates().reshape((-1, gdim))
45 plx,ply = [(dofsV1[:,0]/lx)*2*Nx, (dofsV1[:,1]/ly)*2*Ny]
46 plvec_x,plvec_y = [(dofsV1vec[:,0]/lx)*2*Nx, (dofsV1vec[:,1]/ly)*2*Ny]
47 dofsV1_max, dofsV1vec_max = ((Nx+1)*(Ny+1) + Nx*Ny)*np.array([1,2])
48 # Initialize phi
49 phi = Function( V1 )
50 phi = _comp_lsf(plx,ply,phi,phi_mat,dofsV1_max)
51 # Define Omega = {phi<0}
52 class Omega(SubDomain):
53     def inside(self, x, on_boundary):
54         return between(x[0], (.0,lx)) and between(x[1], (.0,ly)) and phi(x) < 0
55 domains = CellFunction("size_t", mesh)
56 dX = Measure('dx')
57 n = FacetNormal(mesh)
58 # Assemble matrix used to compute descent direction
59 theta,xi = [TrialFunction(V1vec), TestFunction( V1vec)]
60 Av = (1.0*inner(grad(theta),grad(xi)) + 0.1*inner(theta,xi)) * dX\
61      + 1.0e4*(inner(dot(theta,n),dot(xi,n)) * (ds(0)+ds(1)+ds(2)))
62 av = assemble(Av)
63 #----- MAIN LOOP -----
64 while Iter < IterMax and stop_criter == False:
65     # Update and tag Omega = {phi<0}, then solve elasticity system.
66     omega = Omega()
67     domains.set_all(0)
68     omega.mark(domains, 1)
69     dx = Measure('dx')(subdomain_data = domains)
70     U=[0]*len(LoadCase)
71     for k in range(0,len(LoadCase)):
72         U[k] = _solve_PDE(V1vec, dx, ds, eps_er, bcd, mu, lambda, LoadCase[k])
73     # Update cost functional value
74     compliance = 0
75     for u in U:
76         eU = sym(grad(u))
77         compliance += assemble(eps_er * 2.0*mu * inner(eU,eU) * dx(0)\
78                               + eps_er * lambda * tr(eU) * tr(eU) * dx(0)\
79                               + (2.0 * mu * inner(eU,eU) + lambda * tr(eU) * tr(eU)) * dx(1))
80     vol = assemble(VolUnit*dx(1))
81     J[Iter] = compliance + LagVol * vol
82     # ----- LINE SEARCH -----
83     if Iter > 0 and J[Iter] > J[Iter-1] and ls < ls_max:
84         ls += 1
85         beta *= gamma
86         phi_mat,phi = [phi_mat_old,phi_old]
87         phi_mat = _hj(th_mat, phi_mat, lx,ly,Nx, Ny, beta,Txm,Txp,Tym,Typ)
88         phi = _comp_lsf(plx,ply,phi,phi_mat,dofsV1_max)
89         print('Line search iteration : %s' % ls)
90     else:
91         print('***** ITERATION NUMBER %s' % Iter)
92         print('Function value : %.2f' % J[Iter])
93         print('Compliance : %.2f' % compliance)
94         print('Volume fraction : %.2f' % vol/(lx*ly))
95         # Decrease or increase line search step
96         if ls == ls_max: beta0 = max(beta0 * gamma2, 0.1 * beta0_init)

```

```

97         if ls == 0: beta0 = min(beta0 / gamma2, 1)
98         # Reset beta and line search index
99         ls,beta,Iter = [0,beta0, Iter +1]
100        # Compute the descent direction th
101        th = _shape_der(Vlvec, U , eps_er, mu, lambda, dx, av, LagVol)
102        th_array = th.vector().array()
103        th_mat = [np.zeros((Ny+1,Nx+1)),np.zeros((Ny+1,Nx+1))]
104        dof = 0
105        while dof < dofsVlvec_max:
106            if np.rint(plvec_x[dof]) %2 == .0:
107                cx,cy=[int(np.rint(plvec_x[dof]/2)),int(np.rint(plvec_y[dof]/2))]
108                th_mat[0][cy,cx] = th_array[dof]
109                th_mat[1][cy,cx] = th_array[dof+1]
110                dof += 1
111            dof += 1
112        # Update level set function phi using the descent direction th
113        phi_mat_new = _hj(th_mat, phi_mat, lx,ly, Nx,Ny, beta,Txm,Txp,Tym,Typ)
114        if np.mod(Iter,5) == 0: phi_mat_new =
115            _reinit(lx,ly,Nx,Ny,phi_mat_new,Txm,Txp,Tym,Typ)
116        phi_new = _comp_lsf(plx,ply,phi,phi_mat_new,dofsVl_max)
117        phi_old, phi_mat_old = [phi, phi_mat]
118        phi, phi_mat = [phi_new, phi_mat_new]
119        #----- STOPPING CRITERION -----
120        if Iter > 20 and max(abs(J[Iter-5:Iter]-J[Iter-1]))
121            < (2.0/Nx**2)*J[Iter-1]:
122            stop_criter = True
123        #----- Plot Geometry -----
124        if np.mod(Iter,10) == 0 or Iter == 1 or Iter == IterMax or stop_criter
125            == True:
126            pyplot.close()
127            pyplot.contourf(phi_mat,[-10.0,.0],extent = [.0,lx,.0,ly],\
128                cmap=cm.get_cmap('bone'),title='Cantilever')
129            pyplot.axes().set_aspect('equal','box')
130            pyplot.show()
131            pyplot.savefig(results_dir + '/iteration_'+str(Iter)+'.pdf',
132                bbox_inches='tight')
133        return
134    # -----
135    def _solve_PDE(V, dx, ds, eps_er, bcd, mu, lambda, LoadCase):
136        u,v = [TrialFunction(V), TestFunction(V)]
137        eu,ev = [sym(grad(u)),sym(grad(v))]
138        a = eps_er * (2.0*mu * inner(eu,ev) + lambda * div(u) * div(v))* dx(0)\
139            + (2.0 * mu * inner(eu,ev) + lambda * div(u) * div(v)) * dx(1)
140        R = inner(Expression(('0.0', '0.0'),degree=2),v) * ds(2)
141        U,A,b = [Function(V),assemble(a),assemble(R)]
142        delta = PointSource(V.sub(1), LoadCase, -1.0)
143        delta.apply(b)
144        for bc in bcd:
145            bc.apply(A,b)
146        solver = LUSolver(A)
147        solver.solve(U.vector(), b)
148        return U
149    #-----
150    def _shape_der(Vlvec, u_vec , eps_er, mu, lambda, dx, av, LagVol):
151        xi = TestFunction(Vlvec)
152        rv = 0.0
153        for u in u_vec:

```

```

150     divu, divp, eu, Du, Dxi = [div(u), div(xi), sym(grad(u)), grad(u), grad(xi)]
151     rv += assemble(-( eps_er*2*mu*(2*inner( (Du.T)*eu, Dxi) -inner(eu,eu)*divp)
        * dx(0)\
152     +eps_er *lmbda * (2*inner( Du.T, Dxi ) * divu - divu*divu*divp )*dx(0)\
153     +2*mu * (2*inner( eu, Du*Dxi ) - inner(eu,eu)*divp) * dx(1)\
154     +lmbda * (2*inner( Du.T, Dxi ) * divu - divu*divu*divp )*dx(1)\
155     +LagVol*divp* dx(1)))
156     th = Function(Vlvec)
157     solver = LUSolver(av)
158     solver.parameters['reuse_factorization'] = True
159     solver.solve(th.vector(), rv)
160     return th
161     #-----
162     def _hj(v,psi,lx,ly,Nx,Ny,beta,Txm,Txp,Tym,Typ):
163         for k in range(10):
164             Dxm = ( Nx*(np.dot(psi,Txm)) )/lx
165             Dxp = ( Nx*(np.dot(psi,Txp)) )/lx
166             Dyp = ( Ny*(np.dot(Typ,psi)) )/ly
167             Dym = ( Ny*(np.dot(Tym,psi)) )/ly
168             g = 0.5*( v[0]*(Dxp + Dxm) + v[1]*(Dyp + Dym)) \
169                 - 0.5*(np.abs(v[0])*(Dxp - Dxm) + np.abs(v[1])*(Dyp - Dym))
170             maxv = np.max(abs(v[0]) + abs(v[1]))
171             dt = beta*lx / (Nx*maxv)
172             psi = psi - dt*g
173         return psi
174     #-----
175     def _reinit(lx,ly,Nx,Ny,psi,Txm,Txp,Tym,Typ):
176         Dxs = (Nx*(np.dot(psi,Txm)) + Nx*(np.dot(psi,Txp)))/(2*lx)
177         Dys = (Ny*(np.dot(Typ,psi)) + Ny*(np.dot(Tym,psi)))/(2*ly)
178         signum = psi / (np.power(psi**2 + ((lx/Nx)**2)*(Dxs**2 + Dys**2),0.5))
179         dt = 0.5*lx/Nx
180         xx = np.linspace(-lx,lx,Nx+1)
181         yy = np.linspace(-ly,ly,Ny+1)
182         XX,YY = np.meshgrid(xx,yy)
183         for k in range(0,2):
184             Dxm = ( Nx*(np.dot(psi,Txm)) )/lx
185             Dxp = ( Nx*(np.dot(psi,Txp)) )/lx
186             Dyp = ( Ny*(np.dot(Typ,psi)) )/ly
187             Dym = ( Ny*(np.dot(Tym,psi)) )/ly
188             Gp = np.sqrt((np.maximum(Dxm,0))**2 + (np.minimum(Dxp,0))**2 \
189                 + (np.maximum(Dym,0))**2 + (np.minimum(Dyp,0))**2)
190             Gm = np.sqrt((np.minimum(Dxm,0))**2 + (np.maximum(Dxp,0))**2 \
191                 + (np.minimum(Dym,0))**2 + (np.maximum(Dyp,0))**2)
192             g = np.maximum(signum,0)*Gp + np.minimum(signum,0)*Gm
193             psi = psi - dt*(g - signum)
194         return psi
195     #-----
196     def _comp_lsf(plx,ply,phi,phi_mat,dofsVl_max):
197         dof = 0
198         while dof < dofsVl_max:
199             cx,cy = [plx[dof]/2,ply[dof]/2]
200             if np rint(plx[dof]) %2 == .0:
201                 cx,cy = [int(np rint(cx)),int(np rint(cy))]
202                 phi.vector()[dof] = phi_mat[cy,cx]
203             else:
204                 cx,cy = [int(np.floor(cx)), int(np.floor(cy))]
205                 phi.vector()[dof] = 0.25 * (phi_mat[cy,cx] + phi_mat[cy+1,cx]\

```



```

206         + phi_mat[cy,cx+1] + phi_mat[cy+1,cx+1])
207     dof += 1
208     return phi
209 # -----
210 if __name__ == '__main__':
211     _main()
212 # -----

```

## REFERENCES

- [1] Second world congress on computational mechanics the coc algorithm, part ii: Topological, geometrical and generalized shape optimization. *Computer Methods in Applied Mechanics and Engineering*, 89(1):309 – 336, 1991.
- [2] David Adalsteinsson and James A. Sethian. A fast level set method for propagating interfaces. *J. Comput. Phys.*, 118(2):269–277, 1995.
- [3] G. Allaire and O. Pantz. Structural optimization with FreeFem++. *Struct. Multidiscip. Optim.*, 32(3):173–181, 2006.
- [4] Grégoire Allaire, François Jouve, and Anca-Maria Toader. A level-set method for shape optimization. *C. R. Math. Acad. Sci. Paris*, 334(12):1125–1130, 2002.
- [5] Grégoire Allaire, François Jouve, and Anca-Maria Toader. Structural optimization using sensitivity analysis and a level-set method. *J. Comput. Phys.*, 194(1):363–393, 2004.
- [6] Martin Alnæs, Jan Blechta, Johan Hake, August Johansson, Benjamin Kehlet, Anders Logg, Chris Richardson, Johannes Ring, Marie Rognes, and Garth Wells. The fenics project version 1.5. *Archive of Numerical Software*, 3(100), 2015.
- [7] Samuel Amstutz and Heiko Andrä. A new algorithm for topology optimization using a level-set method. *J. Comput. Phys.*, 216(2):573–588, 2006.
- [8] Erik Andreassen, Anders Clausen, Mattias Schevenels, Boyan S. Lazarov, and Ole Sigmund. Efficient topology optimization in matlab using 88 lines of code. *Structural and Multidisciplinary Optimization*, 43(1):1–16, 2010.
- [9] T. Belytschko, S. P. Xiao, and C. Parimi. Topology optimization with implicit functions and regularization. *International Journal for Numerical Methods in Engineering*, 57(8):1177–1196, 2003.
- [10] M. P. Bendsøe. Optimal shape design as a material distribution problem. *Structural optimization*, 1(4):193–202.
- [11] Martin Berggren. A unified discrete-continuous sensitivity analysis method for shape optimization. In *Applied and numerical partial differential equations*, volume 15 of *Comput. Methods Appl. Sci.*, pages 25–39. Springer, New York, 2010.
- [12] Luise Blank, M. Hassan Farshbaf-Shaker, Harald Garcke, Christoph Rupprecht, and Vanessa Styles. Multi-material phase field approach to structural topology optimization. In *Trends in PDE constrained optimization*, volume 165 of *Internat. Ser. Numer. Math.*, pages 231–246. Birkhäuser/Springer, Cham, 2014.
- [13] Blank, Luise, Garcke, Harald, Hassan Farshbaf-Shaker, M., and Styles, Vanessa. Relating phase field and sharp interface approaches to structural topology optimization. *ESAIM: COCV*, 20(4):1025–1058, 2014.
- [14] Blaise Bourdin and Antonin Chambolle. Design-dependent loads in topology optimization. *ESAIM Control Optim. Calc. Var.*, 9:19–48, 2003.
- [15] Martin Burger and Roman Stainko. Phase-field relaxation of topology optimization with local stress constraints. *SIAM Journal on Control and Optimization*, 45(4):1447–1466, 2006.
- [16] Vivien J. Challis. A discrete level-set topology optimization code written in matlab. *Structural and Multidisciplinary Optimization*, 41(3):453–464, 2009.
- [17] Vivien J. Challis, Anthony P. Roberts, and Joseph F. Grotowski. High resolution topology optimization using graphics processing units (gpus). *Structural and Multidisciplinary Optimization*, 49(2):315–325, 2014.
- [18] Marc Dambrine and Djalil Kateb. On the ersatz material approximation in level-set methods. *ESAIM Control Optim. Calc. Var.*, 16(3):618–634, 2010.
- [19] Frédéric de Gournay. Velocity extension for the level-set method and multiple eigenvalues in shape optimization. *SIAM J. Control Optim.*, 45(1):343–367, 2006.
- [20] M. C. Delfour and J.-P. Zolésio. *Shapes and geometries*, volume 22 of *Advances in Design and Control*. Society for Industrial and Applied Mathematics (SIAM), Philadelphia, PA, second edition, 2011. Metrics, analysis, differential calculus, and optimization.
- [21] MC Delfour, Z Mghazli, and J-P Zolesio. Computation of shape gradients for mixed finite element formulation. *LECTURE NOTES IN PURE AND APPLIED MATHEMATICS*, pages 77–94, 1997.
- [22] Leonardo S. Duarte, Waldemar Celes, Anderson Pereira, Ivan F. M. Menezes, and Glaucio H. Paulino. Polytop++: an efficient alternative for serial and parallel topology optimization on cpus & gpus. *Structural and Multidisciplinary Optimization*, 52(5):845–859, 2015.
- [23] J. D. Eshelby. The elastic energy-momentum tensor. *J. Elasticity*, 5(3-4):321–335, 1975. Special issue dedicated to A. E. Green.
- [24] P. Fulmansk, A. Laurain, and J.-F. Scheid. Level set method for shape optimization of Signorini problem. In *MMAR proceedings*, pages 71–75, 2004.
- [25] Piotr Fulmański, Antoine Laurain, Jean-Francois Scheid, and Jan Sokółowski. A level set method in shape and topology optimization for variational inequalities. *Int. J. Appl. Math. Comput. Sci.*, 17(3):413–430, 2007.
- [26] Piotr Fulmański, Antoine Laurain, Jean-François Scheid, and Jan Sokółowski. Level set method with topological derivatives in shape optimization. *Int. J. Comput. Math.*, 85(10):1491–1514, 2008.
- [27] Piotr Fulmansk, Antoine Laurain, Jean-Francois Scheid, and Jan Sokółowski. Une méthode levelset en optimisation de formes. In *CANUM 2006—Congrès National d’Analyse Numérique*, volume 22 of *ESAIM Proc.*, pages 162–168. EDP Sci., Les Ulis, 2008.
- [28] Arun L. Gain and Glaucio H. Paulino. A critical comparative assessment of differential equation-driven methods for structural topology optimization. *Structural and Multidisciplinary Optimization*, 48(4):685–710, 2013.
- [29] P. Gangl, U. Langer, A. Laurain, H. Meftahi, and K. Sturm. Shape optimization of an electric motor subject to nonlinear magnetostatics. *SIAM Journal on Scientific Computing*, 37(6):B1002–B1025, 2015.
- [30] A. Henrot and M. Pierre. *Variation et optimisation de formes*, volume 48 of *Mathématiques & Applications (Berlin) [Mathematics & Applications]*. Springer, Berlin, 2005. Une analyse géométrique. [A geometric analysis].

- [31] David Herrero, Jesús Martínez, and Pascual Martí. An implementation of level set based topology optimization using gpu. In *10th World Congress on Structural and Multidisciplinary Optimization, Orlando, Florida, USA*, pages 1–10, 2013.
- [32] M. Hintermüller and A. Laurain. Optimal shape design subject to elliptic variational inequalities. *SIAM J. Control Optim.*, 49(3):1015–1047, 2011.
- [33] Michael Hintermüller and Antoine Laurain. Multiphase image segmentation and modulation recovery based on shape and topological sensitivity. *J. Math. Imaging Vision*, 35(1):1–22, 2009.
- [34] Michael Hintermüller, Antoine Laurain, and Irwin Yousept. Shape sensitivities for an inverse problem in magnetic induction tomography based on the eddy current model. *Inverse Problems*, 31(6):065006, 25, 2015.
- [35] R. Hiptmair, A. Paganini, and S. Sargheini. Comparison of approximate shape gradients. *BIT*, 55(2):459–485, 2015.
- [36] Laurain, Antoine and Sturm, Kevin. Distributed shape derivative via averaged adjoint method and applications. *ESAIM: M2AN*, 50(4):1241–1267, 2016.
- [37] Kai Liu and Andrés Tovar. An efficient 3d topology optimization code written in matlab. *Structural and Multidisciplinary Optimization*, 50(6):1175–1196, 2014.
- [38] Z. Liu, J.G. Korvink, and R. Huang. Structure topology optimization: fully coupled level set method via femlab. *Structural and Multidisciplinary Optimization*, 29(6):407–417, 2005.
- [39] A. Logg, K.-A. Mardal, and G. N. Wells, editors. *Automated Solution of Differential Equations by the Finite Element Method*, volume 84 of *Lecture Notes in Computational Science and Engineering*. Springer, 2012.
- [40] Junzhao Luo, Zhen Luo, Liping Chen, Liyong Tong, and Michael Yu Wang. A semi-implicit level set method for structural shape and topology optimization. *J. Comput. Phys.*, 227(11):5561–5581, 2008.
- [41] H. P. Mlejnek. Some aspects of the genesis of structures. *Structural optimization*, 5(1):64–69.
- [42] Antonio André Novotny and Jan Sokołowski. *Topological derivatives in shape optimization*. Interaction of Mechanics and Mathematics. Springer, Heidelberg, 2013.
- [43] Stanley Osher and Ronald Fedkiw. *Level set methods and dynamic implicit surfaces*, volume 153 of *Applied Mathematical Sciences*. Springer-Verlag, New York, 2003.
- [44] Stanley Osher and James A. Sethian. Fronts propagating with curvature-dependent speed: algorithms based on Hamilton-Jacobi formulations. *J. Comput. Phys.*, 79(1):12–49, 1988.
- [45] Stanley Osher and Chi-Wang Shu. High-order essentially nonoscillatory schemes for Hamilton-Jacobi equations. *SIAM J. Numer. Anal.*, 28(4):907–922, 1991.
- [46] Masaki Otomori, Takayuki Yamada, Kazuhiro Izui, and Shinji Nishiwaki. Matlab code for a level set-based topology optimization method using a reaction diffusion equation. *Structural and Multidisciplinary Optimization*, 51(5):1159–1172, 2014.
- [47] Danping Peng, Barry Merriman, Stanley Osher, Hongkai Zhao, and Myungjoo Kang. A PDE-based fast local level set method. *J. Comput. Phys.*, 155(2):410–438, 1999.
- [48] Patrick Penzler, Martin Rumpf, and Benedikt Wirth. A phase-field model for compliance shape optimization in nonlinear elasticity. *ESAIM Control Optim. Calc. Var.*, 18(1):229–258, 2012.
- [49] Stephan Schmidt and Volker Schulz. A 2589 line topology optimization code written for the graphics card. *Computing and Visualization in Science*, 14(6):249–256, 2011.
- [50] J. A. Sethian. *Level set methods and fast marching methods*, volume 3 of *Cambridge Monographs on Applied and Computational Mathematics*. Cambridge University Press, Cambridge, second edition, 1999. Evolving interfaces in computational geometry, fluid mechanics, computer vision, and materials science.
- [51] J. A. Sethian and Andreas Wiegmann. Structural boundary design via level set and immersed interface methods. *J. Comput. Phys.*, 163(2):489–528, 2000.
- [52] O. Sigmund. A 99 line topology optimization code written in matlab. *Structural and Multidisciplinary Optimization*, 21(2):120–127, 2014.
- [53] Jan Sokołowski and Jean-Paul Zolésio. *Introduction to shape optimization*, volume 16 of *Springer Series in Computational Mathematics*. Springer-Verlag, Berlin, 1992. Shape sensitivity analysis.
- [54] Kevin Sturm. Minimax Lagrangian approach to the differentiability of nonlinear PDE constrained shape functions without saddle point assumption. *SIAM J. Control Optim.*, 53(4):2017–2039, 2015.
- [55] Kevin Sturm, Michael Hintermüller, and Dietmar Hömberg. Distortion compensation as a shape optimisation problem for a sharp interface model. *Comput. Optim. Appl.*, 64(2):557–588, 2016.
- [56] Akihiro Takezawa, Shinji Nishiwaki, and Mitsuru Kitamura. Shape and topology optimization based on the phase field method and sensitivity analysis. *J. Comput. Phys.*, 229(7):2697–2718, 2010.
- [57] Cameron Talisch, Glaucio H. Paulino, Anderson Pereira, and Ivan F. M. Menezes. Polymesh: a general-purpose mesh generator for polygonal elements written in matlab. *Structural and Multidisciplinary Optimization*, 45(3):309–328, 2012.
- [58] Cameron Talisch, Glaucio H. Paulino, Anderson Pereira, and Ivan F. M. Menezes. Polytop: a matlab implementation of a general topology optimization framework using unstructured polygonal finite element meshes. *Structural and Multidisciplinary Optimization*, 45(3):329–357, 2012.
- [59] Edgardo Taroco and Raúl A. Feijóo. Shape sensitivity analysis and the energy momentum tensor for the kinematic and static models of torsion. *International Journal of Solids and Structures*, 43(7-8):1908 – 1927, 2006.
- [60] N. P. van Dijk, M. Langelaar, and F. van Keulen. A discrete formulation of a discrete level-set method treating multiple constraints. In *Proceedings of 8th World Congress on Structural and Multidisciplinary Optimization*, 2009.
- [61] N. P. van Dijk, K. Maute, M. Langelaar, and F. van Keulen. Level-set methods for structural topology optimization: a review. *Struct. Multidiscip. Optim.*, 48(3):437–472, 2013.
- [62] Michael Yu Wang and Xiaoming Wang. “Color” level sets: a multi-phase method for structural topology optimization with multiple materials. *Comput. Methods Appl. Mech. Engrg.*, 193(6-8):469–496, 2004.
- [63] Michael Yu Wang, Xiaoming Wang, and Dongming Guo. A level set method for structural topology optimization. *Comput. Methods Appl. Mech. Engrg.*, 192(1-2):227–246, 2003.
- [64] Michael Yu Wang and Shiwei Zhou. Phase field: a variational method for structural topology optimization. *CMES Comput. Model. Eng. Sci.*, 6(6):547–566, 2004.

- [65] Tomás Zegard and Glaucio H. Paulino. Toward gpu accelerated topology optimization on unstructured meshes. *Structural and Multidisciplinary Optimization*, 48(3):473–485, 2013.

INSTITUTO DE MATEMÁTICA E ESTATÍSTICA, UNIVERSIDADE DE SÃO PAULO, RUA DO MATÃO, 1010, 05508-090 - SÃO PAULO, BRAZIL

*E-mail address:* laurain@ime.usp.br